Morphology, displacement, and slip rates along the North Anatolian Fault, Turkey

Aurélia Hubert-Ferrari
Laboratoire de Tectonique, IPGP, Paris, France
Department of Geosciences, Princeton University, Princeton, New Jersey, USA

Rolando Armijo, Geoffrey King, and Bertrand Meyer
Laboratoire de Tectonique, Mécanique de la Lithosphère, UMR 7578, CNRS, IPGP, Paris, France

Aykut Barka
Eurasian Earth Sciences Institute, ITU, Ayazaga, Istanbul, Turkey

Received 29 January 2001; revised 8 January 2002; accepted 13 January 2002; published XX Month 2002.

[1] Geological and geomorphological offsets at different scales are used to constrain the localization of deformation, total displacement, and slip rates over various timescales along the central and eastern North Anatolian Fault (NAF) in Turkey. The NAF total displacement is reevaluated using large rivers valleys (80 ± 15 km) and structural markers (Pontide Suture, 85 ± 25 km; Tosya-Vezirköprü basins, 80 ± 10 km). These suggest a Neogene slip rate of 6.5 mm/yr over 13 Myr. The river network morphology shows offsets at a range of scales (20 m to 14 km) across the main fault trace and is also used to estimate the degree to which deformation is localized. At a smaller scale the morphology associated with small rivers is offset by 200 m along the NAF. The age of these features can be correlated with the Holocene deglaciation and a slip rate of 18 ± 3.5 mm/yr is determined. This is consistent with a rate of 18 ± 5 mm/yr deduced independently from the ^{14}C dating of stream terrace offsets. Over the short term, GPS data gives a similar rate of 22 ± 3 mm/yr. All our results tend to show that most of the deformation between the Anatolian and Eurasian lithospheric plates has been accommodated along, or very close to, the active trace of the NAF. The difference between the Neogene and the Holocene slip rate may be due to the recent establishment of the current plate geometry after the creation of the NAF. *INDEX TERMS:* 8107 Tectonophysics: Continental neotectonics; 8158 Tectonophysics: Evolution of the Earth: Plate motions—present and recent (3040); 7230 Seismology: Seismicity and seismotectonics; *KEYWORDS:* North Anatolian Fault, slip rate, total offset, strain localization

1. Introduction

[2] The objective of the present work and *Hubert-Ferrari* [1998] is to study in detail, using geological and geomorphological techniques combined with seismicity data, the behavior of a major continental strike-slip fault, the North Anatolian Fault (NAF). Although such faults must play a role in the deformation of the continental lithosphere, their relative importance with respect to other less localized structures is still discussed. In one extreme case, the continental lithosphere is considered to act as a gravitating and viscous fluid over geological timescales [e.g., *Houseman and England*, 1986; *England and McKenzie*, 1982; *Vilotte et al.*, 1982]. Models based on these assumptions require that the upper seismogenic layer responds passively to distributed tractions at the base of the seismogenic layer [*Jackson*, 1994; *Bournes et al.*, 1998; *Molnar et al.*, 1999]. The other extreme is to consider the lithosphere to be rigid, similar to the oceanic lithosphere. Such models [e.g., *Tapponnier et al.*, 1982] suggest that strike-slip faults should both accommodate a major proportion of the deformation and be highly localized features through the lithosphere [e.g., *Armijo et al.*, 1996; *Meyer et al.*, 1998].

[3] In this paper, we provide data pertinent to a better understanding of this problem for the North Anatolian fault system of Turkey. In particular, we address the question of determining slip rates over various time periods using offset geological and geomorphological markers. The same methods also indicate to what extent the deformation appears to be localized or not. When we combine geodetic data indicating current slip rates with estimates of total fault offsets and seismic behavior, we obtain a clear view of the past and present behavior of the NAF and its deep associated structures.

[4] The right-lateral NAF extends for 1000 km from eastern Turkey to the Aegean Sea in an arc parallel to, and 80–90 km from, the Black Sea coast (Figure 1) [*Ketin*, 1948; *Ambraseys*, 1970; *McKenzie*, 1972; *Barka*, 1992]. The fault trace nearly follows a small circle about a pole in

0148-0227/02/2001JB000393$09.00

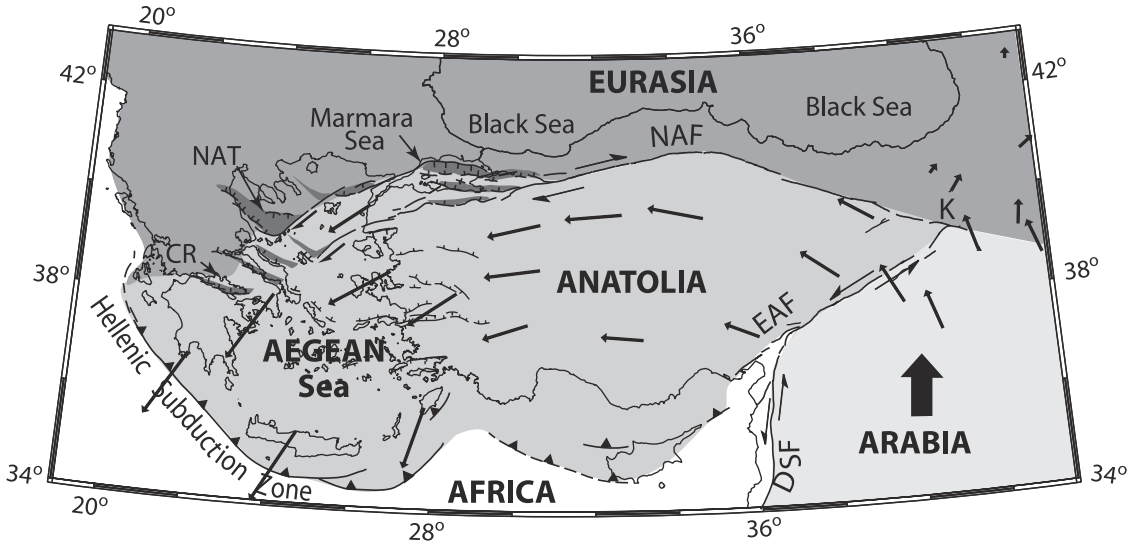

Figure 1. Continental extrusion in the eastern Mediterranean. The Aegean-Anatolia block is escaping westward from the Arabia-Eurasia collision zone toward the Hellenic subduction zone. Current velocity vectors relative to Eurasia in mm/yr (black arrows), using GPS (Global Positioning System) and SLR (satellite laser ranging) are from *Reilinger et al.* [1997]. In the Aegean the westward propagation of the North Anatolian Fault is associated with localized and rapid transtension [*Armijo et al.*, 1996]. CR, Corinth Rift; NAT, North Aegean Trough; NAF, North Anatolian Fault; K, Karliova triple junction; EAF, East Anatolian Fault; DSF, Dead Sea Fault.

the Nile delta that is defined by the GPS data [*McClusky et al.*, 2000]. In its eastern part (Figure 2), the fault strikes N110–120°E for about 500 km and crosscuts a Mesozoic suture. Farther to the west, the NAF bends counterclockwise by about 35° and strikes N75°E for about 300 km, following the intra-Pontide suture zone dating from the Cretaceous to early Eocene. Over much of its length in eastern and central Turkey, the fault is a simple and single structure (Figure 2). In western Turkey, however, the fault splits into two main strands in the Marmara Sea region, and its passage across the Aegean is more complicated (Figure 1) [*McKenzie*, 1978; *Le Pichon and Angelier*, 1981; *Barka and Kadinsky-Cade*, 1988; *Armijo et al.*, 1999]. It forms a broad bathymetric feature known as the Aegean Trough and is related to the enhanced activity of NW-SE extensional basins in Greece. This distribution of deformation has been interpreted either as the motion of two sets of upper crustal slats in relative motions above a viscous lithosphere [*Taymaz et al.*, 1991; *Jackson et al.*, 1992] or as a vast process zone associated with the continued propagation of the NAF in a mantle that retains long-term features [*Armijo et al.*, 1996].

[5] The NAF and the conjugate East Anatolian Fault delimit a block, Anatolia, which is moving westward, pushed by the collision between Arabia and Eurasia (Figure 1). The most recent GPS data suggest a rate of 22 ± 3 mm/yr for the NAF [*Straub et al.*, 1997; *McClusky et al.*, 2000]. Summed seismic moment released over 100–400 years on the fault provides similar but less precise estimates of the slip rate [*Jackson and McKenzie*, 1984, 1988; *Westaway*, 1994]. Estimates of the total offset of the fault vary from 30 to about 100 km [*Koçyigit*, 1989; *Barka and Gülen*, 1988; *Barka*, 1992; *Westaway*, 1994]. The age of the fault appears to be around 13 Ma in its eastern part, resulting in geological rates that have been thought to be between 2 and 10 mm/yr [*Sengör*, 1979; *Barka*, 1992, and references therein]. The reliability and significance of the data on which such estimates are based are discussed below.

[6] The geological and geomorphological markers employed in this study include river valleys, river terraces, and alluvial fans. The biggest rivers in Turkey have valley offsets of tens of kilometers. By comparing to reevaluated geological offsets, we will estimate the total slip on the NAF. On smaller scales, offsets of hundreds of meters are associated with moderate sized valleys, and offsets of meters are associated with individual earthquakes. These offsets, spanning very different spacial scales, are associated with timescales ranging from millions of years to seconds. To examine these morphological features at different scales, we use remote sensing analysis (1:25,000 and 1:100,000 topographic maps, SPOT images, and aerial photographs) combined with fieldwork. This allows us to study the interaction between river networks and the strike-slip movement along the fault, and on this basis we can estimate the degree to which the deformation is localized or distributed. Some morphological features appear to relate to climatic episodes. In particular, many offsets of hundreds of meters can be correlated with the Holocene deglaciation that occurred 10,000–12,000 years ago and thus constrain a fault slip rate over this timescale. At one site, terrace offsets dated using ^{14}C will provide additional information.

[7] Our study is centered on the onland part of the NAF (central and eastern Turkey) where the fault motion is mostly strike-slip (Figure 2). Section 2 is devoted to the study of the relationship between the seismic behavior, and the step overs and bends, of the North Anatolian fault system. This provides a good introduction to the general characteristics of the fault trace. We also discuss the

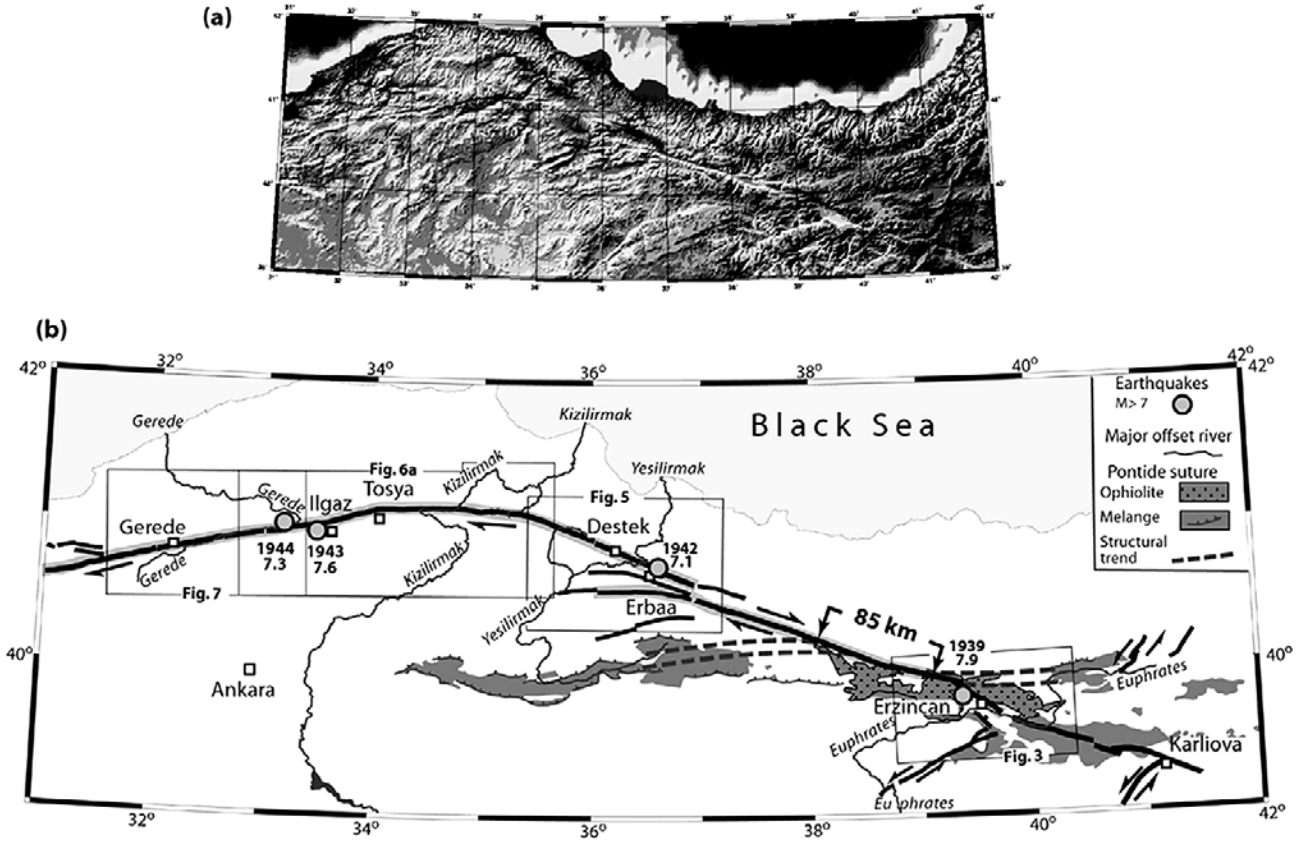

Figure 2. Tectonic setting. (a) Shaded topography (GTOPO 30, U.S. Geological Survey). The trace of the central and eastern segments of the NAF appears clearly. (b) The trace of the NAF with the twentieth century earthquakes sequence (the corresponding ruptures extension are in shading). The apparent right-lateral offsets of large river valleys are clearly visible. The Pontide suture (structural trend, ophiolite massif, and melange outcrop) of upper Cretaceous to Eocene age appears to be right-laterally offset by about 85 km [*Seymen*, 1975; *Sengör et al.*, 1985; *Bingöl*, 1989]. We have enclosed the areas studied in details in the paper in boxes.

possible crustal scale complexities in the fault geometry. We then turn to the main points of the paper: in section 3 we study the geological and large river offsets to reevaluate the NAF total displacement, and in section 4 we consider the offset morphology at smaller scales in the Ilgaz Mountains (main fault bend). We have studied this latter region in greater detail, and it is particularly well-suited to illustrate the methods we use. Similar and complementary material on other sites is included in Appendix A. We conclude the paper with a detailed discussion of our results, and we give a sketch of a possible evolution of the NAF over the long term.

2. Seismicity and Geometry Along the NAF

[8] During the twentieth century, a series of strike-slip earthquakes of magnitude greater than 7 have ruptured most of the NAF. The main events in the eastern and central part of the fault occurred in 1939, 1942, 1943, and 1944 in a westward propagating strike-slip sequence and ruptured long stretches (50–350 km) of the NAF (Figure 2b) [*Ketin*, 1969; *Ambraseys*, 1970]. The last events of this series ruptured the NAF in its western part in 1957–1967–1999 [*Ambraseys and Zatopek*, 1969; *Öcal*, 1959; *Stein et al.*, 1997; *Nalbant et al.*, 1998; *Hubert-Ferrari et al.*, 2000]. We use the mapped earthquake ruptures [*Ambraseys*, 1970] combined with satellite data analysis to characterize the active fault trace of the NAF in its eastern and central part (Figure 2). Though the NAF is a simple and single feature over much of its length (Figure 2a), important secondary active structures are associated with major bends or step overs in the fault trace, and it is possible to speculate about the extent to which these complexities in the fault geometry are superficial or affect most of the crust. To do so, we examine the relationship between the rupture extremities, the epicenter locations and the fault geometry. We first focus on the two main releasing step overs, the Erzincan and Erbaa basins in the eastern part of the NAF arc, and then on the main restraining fault bend where the NAF veers by about 35° in its central part (Figure 2b).

[9] The NW-SE striking Erzincan basin appears to be a major step over along the NAF [*Sengör*, 1979; *Aydin and Nur*, 1982; *Hempton and Dunne*, 1984; *Barka and Gülen*, 1989]. The geometry of the fault system in this region is shown on Figure 3. Two main fault segments, with similar strike (N110°E), enter at the NW and SE extremities of the

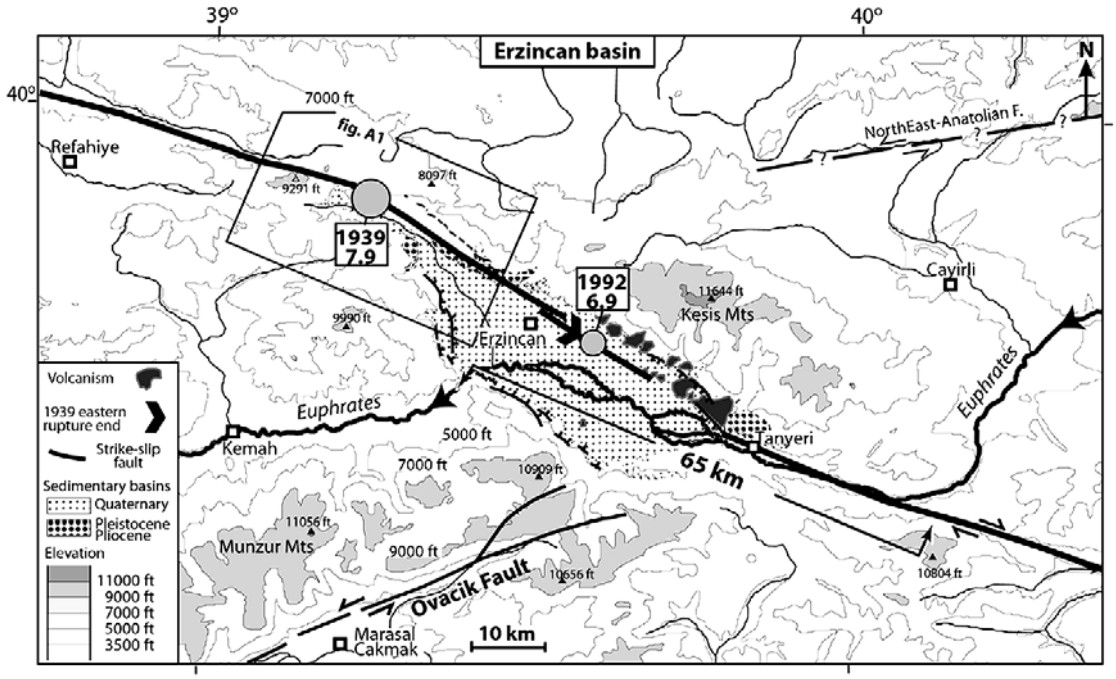

Figure 3. The Erzincan basin region (see location in Figure 2b). This 50-km-long asymmetric depression is bordered to the NW and SE by two left-stepping segments of the NAF that are linked by a 100-km-long central segment crossing the basin. The 1939 earthquake epicenter is located near the restraining bend to the NW and ruptures both the northwest and the central segments. The 1992 earthquake ruptured the central segment farther to the east. Normal faulting and volcanism in the eastern part of the basin may be the consequence of the releasing fault geometry between the central and the southeast NAF segments. Left-lateral movement on the Ovacik fault to the south may contribute to the extension in the SW side of the basin. The valley of the Euphrates River is offset 65 km across the NAF. The topography (in feet) is from tactical pilotage charts at 1:500,000 scale. The location of Figure A1 is shown; the exact locations of the villages Mihar and Bahik are indicated in Figure A1.

basin and are linked by a third 100-km-long fault segment having a different strike (N125°E). The latter follows the northern edge of the basin and disappears eastward under the alluvium. The SE extremity of the basin also marked the termination of the left-lateral, ENE striking, Ovacik fault [*Arpat and Şaroglu*, 1972; *Barka and Gülen*, 1989; *Fuenzalida et al.*, 1997]. This complex fault geometry implies that the Erzincan basin is not a simple pull-apart [*Barka and Gülen*, 1989; *Fuenzalida et al.*, 1997]. It also generates high local stresses in the basin, that may be released by small local events like the 1992 M = 6.9 Erzincan earthquake [*Fuenzalida et al.*, 1997] (Figure 3). The seismic behavior of the NAF appears to be decoupled on both sides of the Erzincan depression. East of the basin, the only known major earthquake occurred in 1784 [*Ambraseys*, 1989], while to the west the NAF has ruptured several times in well-defined sequences [*Ambraseys*, 1970; *Ambraseys and Finkel*, 1988]. This suggests that the Erzincan basin is a major discontinuity along the NAF and impedes ruptures. This is well illustrated by the 1939 Erzincan earthquake, which is the first and largest (M = 7.9) earthquake of the twentieth century sequence (Figure 2b). The epicenter was located near the western extremity of the basin (Figure 3) [*Deweys*, 1976], where the fault bends by 15. The associated rupture had up to 7.5 m of right-lateral displacement [*Koçyigit*, 1989; *Barka*, 1996] and propagated about 280 km to the west toward the Erbaa basin, but only about 80 km to the east into the Erzincan basin (Figures 2b and 3) [*Deweys*, 1976; *Barka and Kadinsky-Cade*, 1988]. The amount of deformation seems to have been similar on both sides of the fault bend. Sag ponds (Figure 4a) and shutter ridges that deviate stream channels (Figure 4b), which are located west and east of the bend area, have dimensions compatible with 6 m of right-lateral slip. There is no evidence to suggest that the bend impeded slip. We thus infer that the NAF forms a continuous fault surface at depth through the bend (see Appendix A for further discussion). Unlike the basin itself, the bend thus does not significantly interfere with propagation of major earthquakes.

[10] The same kind of observations can be made at the Erbaa basin, where the 1939 Erzincan earthquake as well as another major (M = 7.6) earthquake that occurred in 1943 terminated [*Ketin*, 1948; *Ambraseys*, 1970]. This pull-apart basin results from a 10 km releasing step between two linear N110°E striking fault segments (Figures 2b and 5a) [*Allen*, 1975]. The 1939 event is diverted from the main fault system by the Erbaa basin to the Ezinpazari fault to the south, where it continued to rupture for a farther 65 km (Figure 5a) [*Barka*, 1996]. This secondary fault is part of the horsetail formed by the Esencay, the Ezinpazari, and the Almus faults [*Sengör and Barka*, 1992; *Tartar et al.*, 1995; *Bozkurt and Koçygit*, 1996]. These faults strike parallel to

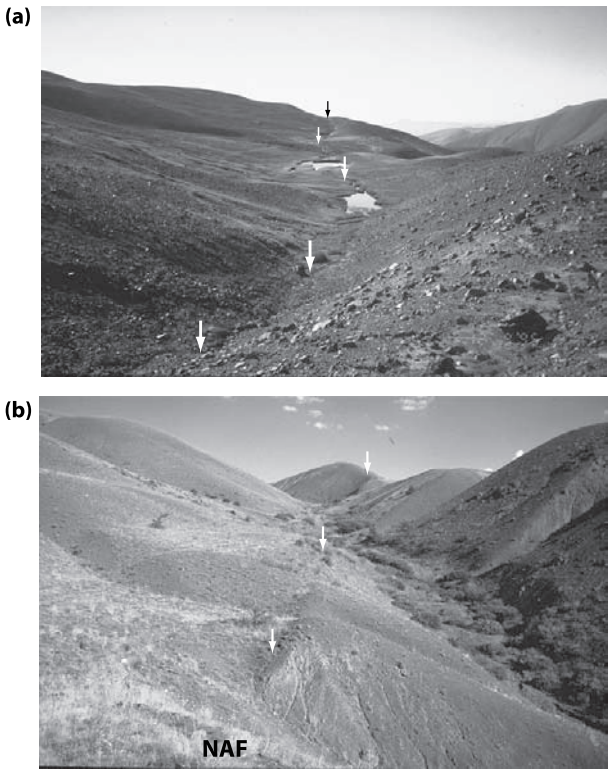

Figure 4. Views of the surface break associated with the 1939 earthquake (see Figure A1 for exact locations). (a) Sag ponds and pull-aparts west of the fault bend, to the west of Mihar. (b) Shutter ridges deviating streams east of the fault bend, to the west of Bahik. The dimensions of sag ponds, pull-aparts, shutter ridges, and stream offsets are all consistent with 6 m of right-lateral slip on both sides of the fault bend [*Barka*, 1996].

the Mesozoic structures. Together with the basin itself, they may be inherited from the initial fault propagation process, at the time before the main fault had established its present trace. Local strain due to the Erbaa basin fault geometry was released in 1942 by a magnitude 7.1 event that ruptured across the northern side of the pull-apart and some distance into the hills to the east [*Ambraseys*, 1970]. The above observations suggest that the Erbaa pull-apart, like the Erzincan basin, is a discontinuity along the fault. In both cases, major earthquake ruptures are impeded by these structures, which suggests that the superficial geometry of the fault should extend to depth in the crust. However, the Erbaa structure shall extend to shallower depth than the Erzincan structure, since earthquake sequence are completely impeded across the latter and not across the former.

[11] The situation is different in the main restraining bend of the NAF, where its trace veers by about 35 in two steps near Vezirköprü and Tosya (Figure 6). This region was the locus of the 1943 M = 7.6 Tosya earthquake that extended over 280 km across the fault bend (Figure 2b) [*Ambraseys*, 1970; *Barka and Kadinsky-Cade*, 1988]. The region was also the locus of one of the largest earthquakes in central Turkey that occurred in 1668 and was reported to have ruptured along a similar but even longer fault stretch [*Ambraseys and Finkel*, 1988]. The fact that these two major events ruptured through the fault bend implies that in this region, unlike in the pull-aparts farther east, the bend does not inhibit rupture. Thus it is reasonable to suppose that strike-slip deformation is localized at depth along a well-defined fault surface which continuity is little perturbed by the bending of the fault. In 1944, an important M = 7.3 event, which continued the sequence 1939–1942–1943, occurred farther west along a straighter part of the NAF, with a displacement of 1 to 3.5 m (Figure 7) [*Ambraseys*, 1970; *Barka*, 1996]. Interestingly, the boundary between the 1943 and 1944 events is located at the merging of the main fault system with the thrust structures associated with the Cerkes basin. To the west, the rupture ended at another fault complexity, the Almacik block [*Ambraseys*, 1970; *Barka*, 1996; *Armijo et al.*, 1999]. Note that the main NAF fault bend is much sharper than the ideal plate boundary geometry that should follow a small circle about a pole near the Sinai [*Hubert-Ferrari*, 1998; *McClusky et al.*, 2000]. This restraining geometry implies that active thrusting should occur locally in addition to strike-slip faulting. The M = 6.9 Cerkes earthquake in 1951 [*Ambraseys*, 1970; *Barka and Kadinsky-Cade*, 1988], ruptured the NAF and the thrust fault bounding the Cerkes basin (Figure 6a) [*Ambraseys*, 1970]. Even if its focal mechanism was mainly strike slip [*McKenzie*, 1972], this earthquake is likely to have partly released the strain induced by the bending of the fault. It is also consistent with geological and geomorphological observations that suggest active compressional deformation in the Ilgaz Mountains area [*Barka*, 1984; *Barka and Hancock*, 1984; *Över et al.*, 1993; *Andrieux et al.*, 1995; *Barka*, 1992].

[12] In summary, the Erzincan basin, and to a lesser degree the Erbaa basin, are two major step overs that apparently play an important role in controlling the rupture extension of large earthquakes (M > 7.5). The Erzincan structure completely impedes the seismic ruptures and must extend to a depth greater that the seismogenic layer, whereas the Erbaa pull-apart should not extend so far. Such features may be inherited from the mechanical processes that occurred at the time of the birth and propagation of the NAF in the Eurasian plate. Unlike these offsets, the main bends along the NAF (in Erzincan or in its central part) do not stop rupture propagation of large earthquakes. This implies that the fault at depth in these regions has greater continuity. Note also that the fault arc do not follow exactly a "small circle" but is parallel to the Black Sea coast line. This suggests that the presence of this oceanic lithosphere may have play an important role during the establishment of the NAF in the Eurasian lithosphere.

3. Total Displacement and Long-Term Slip Rates

3.1. Geological Offsets and the Age of the Fault

3.1.1. Earlier works

[13] Earlier work describes the offset of a large Mesozoic structure that the fault crosses obliquely at its eastern end. Known as the Pontide suture (Figure 2b) [*Seymen*, 1975; *Bergougnan*, 1975; *Sengör et al.*, 1985], this ophiolitic assemblage extends over hundreds of kilometers across the fault and results mainly from the obduction/collision between the Pontide island arc to the north and the Anatolide/Tauride platform to the south during the Upper Cretaceous to lower Eocene [*Sengör et al.*, 1985; *Yilmaz*, 1985;

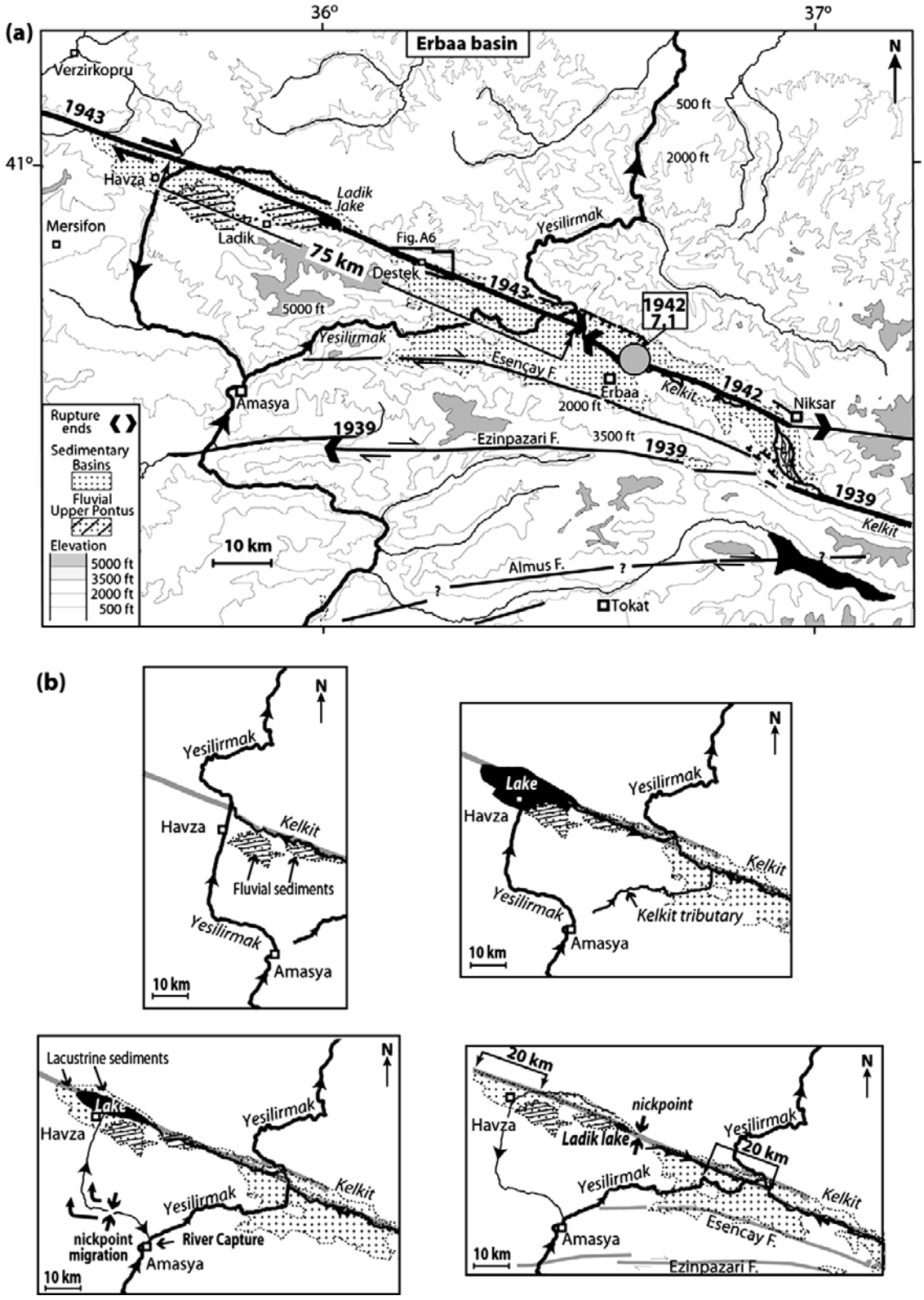
(a)
36°
37°
41°
Erbaa basin
N
Verzirkopru
1943
Havza
Ladik Lake
Mersifon
Ladik
Fig. A6
75 km
Destek
1943
Yesilirmak
500 ft
2000 ft
5000 ft
Yesilirmak
1942
7.1
Esençay F.
Erbaa
Kelkit
1942
Niksar
Amasya
2000 ft
1939
Ezinpazari F.
3500 ft
1939
1939
Kelkit
Rupture ends
Sedimentary Basins
Fluvial Upper Pontus
Elevation
5000 ft
3500 ft
2000 ft
500 ft
10 km
Almus F.
?
?
?
Tokat
(b)
N
Yesilirmak
Havza
Kelkit
Fluvial sediments
Yesilirmak
Amasya
10 km
N
Lake
Yesilirmak
Havza
Kelkit
Yesilirmak
Kelkit tributary
Amasya
10 km
Lacustrine sediments
N
Lake
Yesilirmak
Havza
Yesilirmak
Kelkit
nickpoint migration
River Capture
Amasya
10 km
20 km
N
nickpoint
Havza
Ladik lake
Yesilirmak
20 km
Yesilirmak
Kelkit
Esencay F.
Amasya
10 km
Ezinpazari F.

Yilmaz et al., 1997; *Okay and Sahinturk*, 1997]. Near Erzincan, the ophiolitic body appears north of the fault and is found again south of the fault about 80 to 90 km farther west [*Bingöl*, 1989; *Okay and Sahinturk*, 1997]. This offset is consistent with that of the structural trend of the associated melange (Figure 2b) [*Sengör et al.*, 1985]. However, the uncertainty of this estimate is large, and much lower or higher values, ranging from 30 to 120 km, have been proposed in the literature [*Seymen*, 1975; *Bergougnan*, 1975; *Sengör et al.*, 1985; *Yilmaz et al.*, 1993]. Disagreement is apparently due to the poor resolution of mapped structures associated with the suture, which are obscured by young volcanism and sediment. Moreover, the fact that these structures have been rotated and sheared into slices near the fault may have added to confusion. Nevertheless, we estimate that a conservative value of 85 ± 25 km is consistent with the broad-scale offset structure illustrated in Figure 2b. Since the Pontide suture extends over hundreds of kilometers across the fault, its maximum offset also constrains the total amount of extrusion of the Anatolian plate, independently of the fact that minor faults or more continuous penetrative strain may have accommodated a fraction of the slip.

[14] Other large-scale, but more localized, structural markers have been documented by *Armijo et al.* [1999] in the western NAF, around the Sea of Marmara pull-apart. They documented a total displacement along the two main strands of the NAF of about 85 km in 5 Myr.

[15] No other large-scale structural offset has been documented to our knowledge prior to the present work. In the central part of the NAF, small-scale geological offsets ranging from 25 to 30 km are described across sedimentary basins [*Barka and Hancock*, 1984; *Barka and Gülen*, 1989] and eroded volcanic outcrops [*Şaroglu*, 1988; *Koçyigit*, 1989, 1990]. Unfortunately, the age and more importantly the initial shape and structure of the basins and volcanic outcrops have not been well constrained. These values of 25–30 km should be considered as minimum estimates of the total displacement across the fault.

[16] The NAF is thought to have initiated in early late Miocene time, about 13 Ma in the eastern Turkey [*Sengör et al.*, 1985], soon after the beginning of the continental collision between the Arabian and Eurasian plate and the rise of the eastern Anatolian Plateau (~15 Ma). This age estimate is mainly based on the age of the base of lacustrine sediments infilling sedimentary basins along and around the NAF [*Irrlitz*, 1972; *Rogl and Steininger*, 1983; J.-C. Guezou, personal communication, 2001]. The age of the fault in its western part is thought to be younger (5 Ma) [*Armijo et al.*, 1999]. If this is correct, the fault must have propagated westward over times spanning several million years, and the long-term slip rate must vary between 6.5 mm/yr in the east and 17 mm/yr in the west. This observation will be discussed later in the light of the results presented in this paper.

3.1.2. Sheared Synclines in the Ilgaz Mountains

[17] In the central part of the NAF we mapped the folding associated with three large intramountain basins (Tosya, Ilgaz, and Cerkes). These basins are bounded (Figures 6a and 6b) to the north by southeast verging thrusts underlying N70–80°E striking anticlines (Figure 6b) [*Barka*, 1984]. The thrust folds are about 30 km long and have an average strike consistent with the dextral slip on the NAF. The three basins are filled by lacustrine and fluvial sediments of the Pontus formations [*Barka and Hancock*, 1984; *Barka*, 1992]. A Plio-Pleistocene age (4–2 Ma) for the Pontus formation is inferred from the dating of Chariophystes and Ostracodes [*Över*, 1996] in the Tosya basin and of mammals [*Ünay and de Bruijn*, 1998]. However, the bottom of the sedimentary section is considered to be older than 5 Ma [*Barka and Hancock*, 1984] and locally lie on top of 8.5 Ma volcanic rocks [*Adyaman*, 2000; J.-C. Guezou, personal communication, 2001]. Folding involves both the pre-Neogene basement and the unconformable Pontus formation [*Barka and Hancock*, 1984; *Över et al.*, 1993; *Andrieux et al.*, 1995], which suggests that it started 5–8.5 Ma. The three folds and associated basins have a similar structure, but their respective morphology is different. The elevations of the basins decreases eastward from 1600 m for the Cerkes basin to 900 m for the Tosya basin, while the anticline elevation increases to the east (1783, 1960, and 2285 m in Cerkes, Ilgaz, and Tosya anticlines, respectively). The eastward increases in structural relief shows that the cumulative deformation associated with these structures increases eastward toward the main fault bend (Figures 6a and 6b).

Figure 5. (opposite) The Erbaa pull-apart basin (see location in Figure 2b). (a) This rectangular depression, filled by lacustrine and fluvial sediments of the Pontus formation, results from a 10-km releasing step between two linear N110°E striking fault segments of the NAF. The Esencay, Ezinpazari, and Almus faults splay with a horsetail geometry, west from the southeast segment of the NAF. The Erbaa basin was the locus of the 1942 earthquake epicenter, and the 1939 and 1943 ruptures terminated there. The Yesilirmak river valley can be interpreted to be offset 75 km by the NAF (see Figure 5b). Destek area shown in Figure A6 is outlined. Topography as in Figure 3. (b) Sketch of a possible scenario for the interaction between the Yesilirmak river and the NAF. (top left) Before the NAF propagation took place, the Yesilirmak and Kelkit rivers may have deposited a large amount of fluvial sediments along their courses, whose present remnants are mapped. This figure has been obtained by 75 km of left-lateral offset along the NAF, starting from the present-day setting displayed in Figure 5a. (top right) When the elongation of the Yesilirmak reaches a certain threshold, the stream power decreases, which could trigger river capture (see section 4 for complementary discussion). The capture may have been enhanced by the presence of the Havza pull-apart lake whose mapped extension corresponds to the Havza-Ladik lacustrine deposits displayed in Figure 5a. (bottom left) After the river capture, the lake should recess, and lacustrine sediments and the new course of the Yesilirmak should begin to be offset. A nickpoint delimiting tributaries flowing northward or southward would migrate upstream toward its present position near the Ladik Lake. (bottom right) Present-day morphology. A rough match is found between the 20-km offsets of the lacustrine sediments in Havza and of the Yesilirmak river in the Erbaa basin.

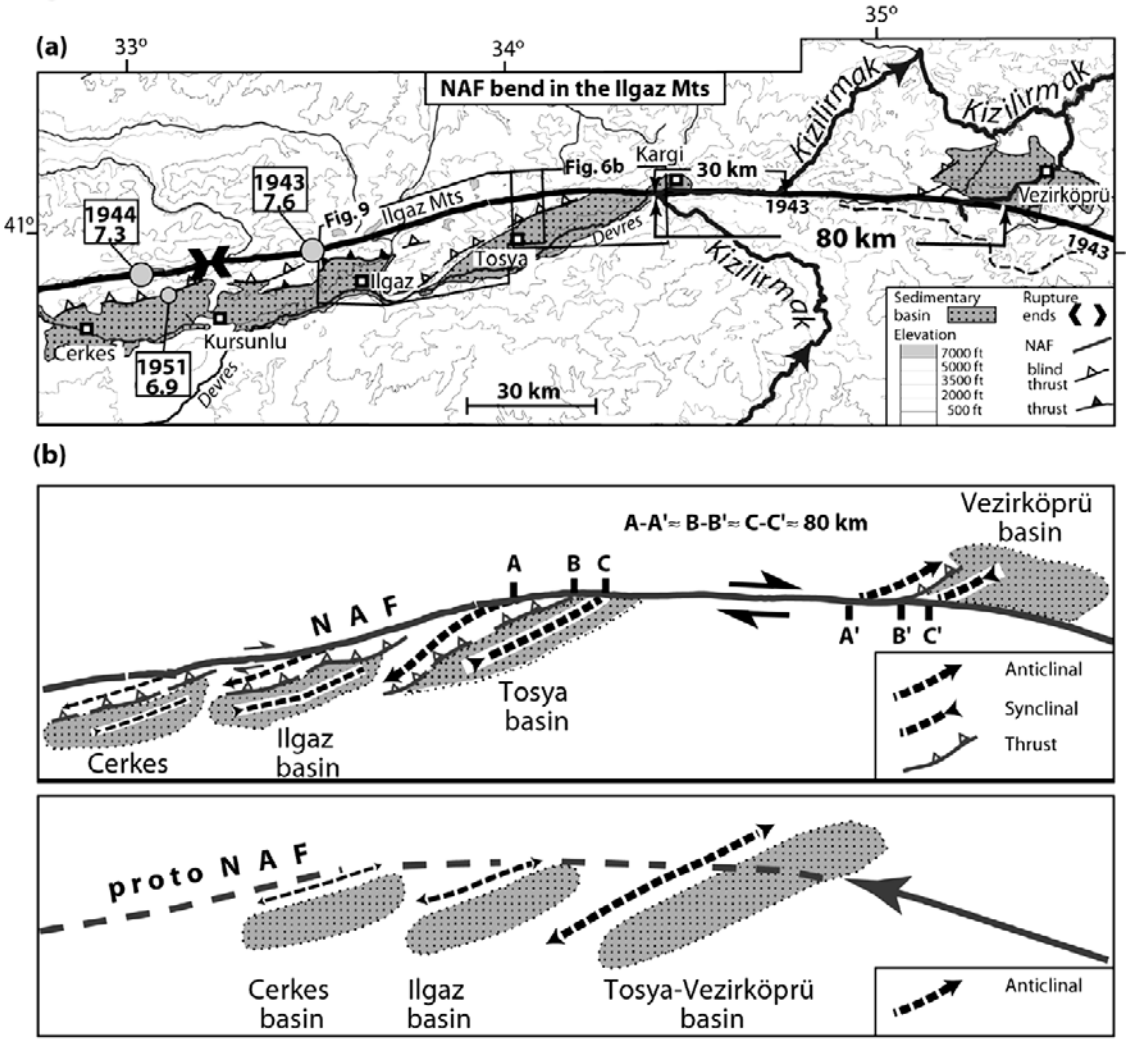
(a)
33°
34°
35°
41°
NAF bend in the Ilgaz Mts
Kizilirmak
Kizilirmak
Kargi
Fig. 6b
30 km
1943
Vezirköprü
1943
7.6
1944
7.3
Fig. 9
Ilgaz Mts
Devres
80 km
1943
Tosya
Ilgaz
Kizilirmak
Sedimentary basin
Rupture ends
Elevation
7000 ft
5000 ft
3500 ft
2000 ft
500 ft
NAF
blind thrust
thrust
Cerkes
Kursunlu
1951
6.9
Devres
30 km
(b)
A-A'≈ B-B'≈ C-C'≈ 80 km
Vezirköprü basin
A
B
C
A'
B'
C'
N A F
Tosya basin
Cerkes
Ilgaz basin
Anticlinal
Synclinal
Thrust
proto N A F
Cerkes basin
Ilgaz basin
Tosya-Vezirköprü basin
Anticlinal
(c)

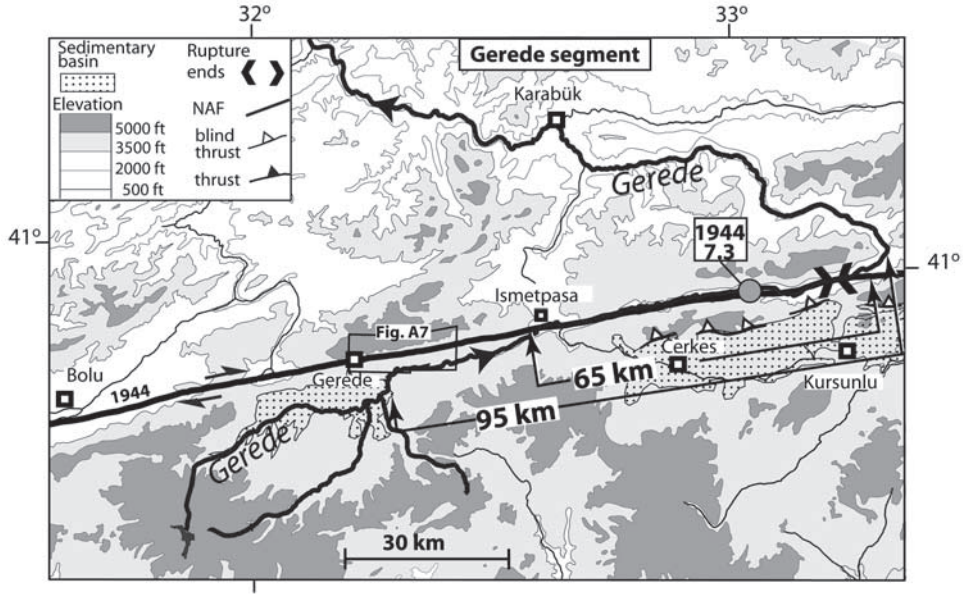

Figure 7. The straight Gerede segment of the NAF (see location in Figure 2b). The right-lateral offset of Gerede river valley is 65–95 km. Labeled frames identify the location of Figure A7. Topography as in Figure 3.

[18] The Tosya basin and anticline are truncated to the north by the NAF. This is clearly seen in the topography and in the SPOT image (Figures 6a and 6c). Two sedimentary basins on the north side of the fault could correspond to its northward continuation. One is the small (10 km by 3 km), Kargi basin, close to the Tosya basin. The other is the larger (50 km by 15 km), Vezirköprü basin, located 80 km to the east. While the Kargi basin is filled with Quaternary sediments, too young to match those of the Tosya basin, the Vezirköprü basin is filled by fluvial and lacustrine sediments having an upper Miocene to Pleistocene age [*Dirik*, 1993] matching well the Tosya basin sediments.

[19] Its seems plausible that the Tosya and Vezirköprü basins were joined before the fault slip separated them. This is further supported by the following facts. First, the western edge of the Vezirköprü basin is bounded by a small mountain range that seems to match the Tosya anticline. Second, the present river network that flows northward into the Vezirköprü basin is too small to account for the total amount of alluvial sediments. However, if the Kizilirmak river, that nowadays crosses the fault near the eastern edge of the Tosya basin, originally traversed both basins, this would account both for the quantity and form of the Vezirköprü sediments. In this view, the two truncated synclinal basins were formed before being cut and right-laterally offset by about 80 km by the NAF, which is the distance between the Tosya and Vezirköprü basins (Figure 6b). The offset uncertainty is about 10 km because the eroded western edge of the Vezirköprü basin is not as well defined as the northeast edge of the Tosya basin.

[20] More generally, the folds can be interpreted as resulting from the NAF propagation process into the area at 5–8.5 Ma. The mechanical situation would be similar to that proposed to have created folds of the Gelibolu peninsula in the Marmara Sea area at about 5 Ma [*Armijo et al.*, 1999]. The two truncated Tosya and Vezirköprü synclinal basins were formed by stresses ahead of the approaching western extremity of the NAF as it bends and forms an arc parallel to the Black Sea coast (Figure 6b). Once formed, the basins were then cut by the fault to give the present-day

Figure 6. (opposite) The main bend region of the NAF in the Ilgaz Mountains (see location in Figure 2b). (a) The fault bends by about 20° at the western end of the Vezirköprü basin and by 15° farther west near Tosya. To the west of the bend, the NAF runs through the Ilgaz Mountains, which are bounded southward by SSE verging, en echelon, thrusts. These thrusts make the northern borders of the Cerkes, Ilgaz, and Tosya basins. The latter are filled with continental sediments of the Pontus formation (late Miocene–early Pleistocene age [*Barka and Hancock*, 1984]) and are drained by the Devres river. The Kizilirmak valley is right-laterally offset 30 km across the fault [*Barka and Hancock*, 1984] but may have flowed initially through the Vezirköprü basin. This idea is supported by the fact that the present catchment of the rivers flowing through the basin (marked by a dashed line) have a too small extension to have brought the sediments infilling it. The epicenters of the 1943, 1944 (location ±20 km), and 1951 earthquakes are indicated. Topography as in Figure 3. Labeled frames identify the location of Figures 6b and 9. (b) The sketch of the thrusts and basins displaying the possible 80-km offset of the Tosya-Vezirköprü basins. (top) Present-day geometry. (bottom) Before the NAF propagation took place, the folds and associated basins are created by stresses ahead of the approaching western extremity of the NAF as it bends. Once formed, they were cut by the NAF to give the present-day offset between the Tosya and Vezirköprü basins displayed in Figure 6b, bottom. Additional sediments may have been deposited in the Vezirköprü basin before the Kizilirmak capture. (c) SPOT image of the northeastern end of the Tosya basin, truncated by the NAF (see arrows for the NAF trace).

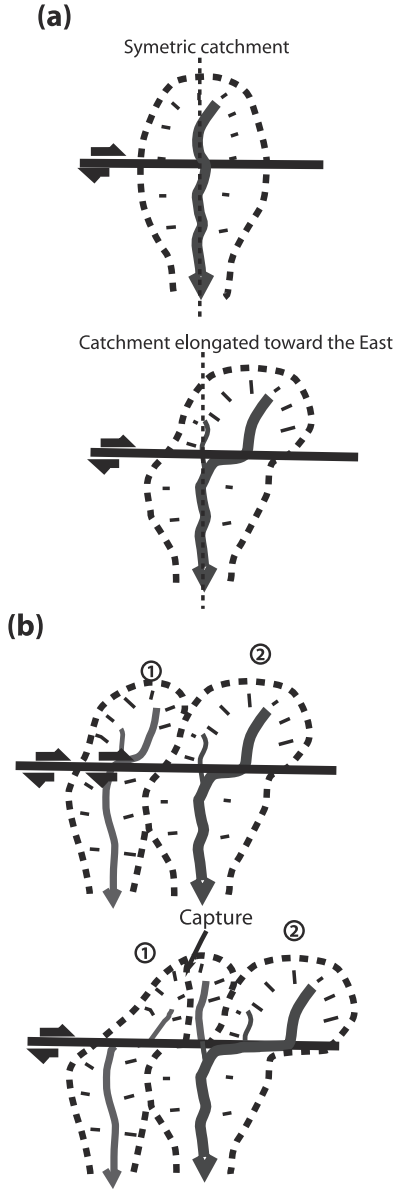

Figure 8. Possible evolution of river catchments by right-lateral slip along a fault. (a) A catchment develops a wrenched shape with increasing slip on the fault. (b) Fault displacement favors valley capture by adjacent streams.

offset between the Tosya and Vezirköprü basins. At some point during that period, the Kizilirmak river changed course as a consequence of capture and the original course became the minor tributary that now crosses the Vezirköprü basin. Because of the present-day geometry of the sharp restraining bend of the NAF, shortening must continue into present times as in the Dardanelles.

3.2. Large River Valley Offsets and Long-Term Slip Rates

[21] Large river valley offsets can be used to further constrain the total displacement along the NAF. River valleys are markers that tend to be deflected by active strike-slip faulting (Figure 8) [*Wallace*, 1968; *Gaudemer et al.*, 1989; *Lacassin et al.*, 1998; *Replumaz et al.*, 2001]. However, these markers must be used with caution because the age of a river is unknown and may not pre-date fault motion, and river capture tends to bypass offsets as time passes (Figure 8b). For both of these reasons, river offsets generally underestimate total slip [*Lacassin et al.*, 1998]. To reduce the sources of errors, we use as markers large rivers, that have large drainage areas and are usually more long-lived than the features they cross. We also examine the present river channel geometry, its tributaries and the associated sedimentary basins, to map possible paleochannels that would indicate capture.

[22] In eastern and central Turkey, four main large rivers cross the NAF between longitudes 30°E and 42°E (Figure 2b). The Euphrates river in the east flows southeast from the eastern Pontide Range to the Persian Gulf, whereas the Yesilirmak, Kizilirmak, and Gerede rivers flow northward from central Turkey to the Black Sea.

3.2.1. The Euphrates river

[23] After rising in the eastern Pontide mountain range, the Euphrates river flows SSW to cross the NAF in the Erzincan basin (Figures 2b and 3). At the fault, it veers by 90 to flow ENE along the fault before entering the Erzincan basin. Near the town of Erzincan, it leaves the depression through a NE-SW narrow outlet where the normal faults bounding the southern edge of the basin change strike by about 25 (Figure 3). The offset of the valleys associated with the river course suggests a cumulative right-lateral displacement of 65 km similar to the estimates in previous studies [*Barka and Gülen*, 1989; *Gaudemer et al.*, 1989].

3.2.2. The Yesilirmak river

[24] The Yesilirmak river flows south of the NAF toward the NE, enters into the Erbaa basin along its SW rim, and then defines a right-lateral offset a few kilometers long along the NAF (as reported by *Barka* [1984] and in Figures 2b and 5a). To the north of the fault trace, it turns N100°E for about 10 km and then resumes flowing toward the NNE. The small offset of the Yesilirmak river cannot correspond to the total offset of the NAF. It is much more likely that the present course of the river is the result of a river capture. A possible scenario is illustrated in Figure 5b. A tributary of the Kelkit river could have intercepted and captured the river main course near the town of Amasya. Such a capture may have been favored by motion along the Esencay fault. A possible paleochannel of the Yesilirmak river is the stretch of river between Amasya and Havza. This hypoth-

Table 1. Large Offsets Measured Across the North Anatolian Fault[a]

	Offset Structures	Offset Valleys	Mean Amount, km
Eastern NAF	Pontide suture		85
		Euphrates	65
Central NAF	Tosya basin		80
		Yesilirmak	75
		Kizilirmak	80
		Gerede	80
Western NAF	Dardanelles folds		70
	Eocene volcanics		50
	Marmara pull-apart		85
		Sakarya	85

[a] Obseravations for the western NAF are from *Westaway* [1994] and *Armijo et al.* [1999].

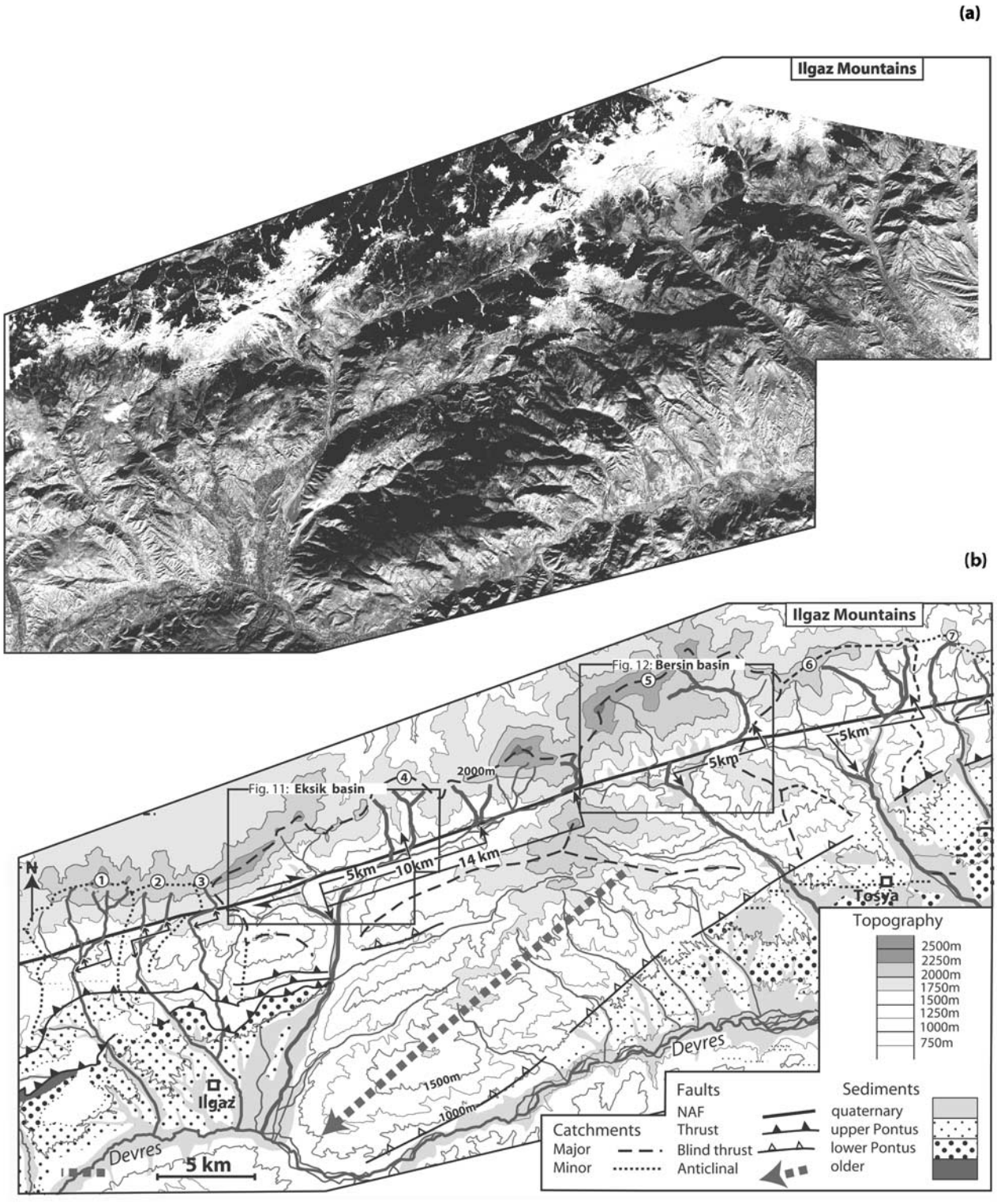

Figure 9. The NAF in the Ilgaz Mountains (see location in Figure 2b). (a) Panchromatic SPOT image (10-m resolution). (b) Morphology of the same area shows the offset drainage along the trace of the NAF. Valley offsets across the NAF range from 1 to 14 km. The amount of lateral offset correlates with the surface area of the catchments: rivers with larger catchments (>100 km^2) are offset by about 5 km, while those with smaller catchments (<50 km^2) are offset by about 1–2 km. The latter are marked by small arrowheads without labels. The catchments are numbered 1 to 7. Frames for the location of Figures 11 and 12 are shown. Anticlines and thrusts north of the Tosya and Ilgaz basins are from *Barka* [1984]. Topography is from 1:100,000 maps (Army Geographical Service of Turkey).

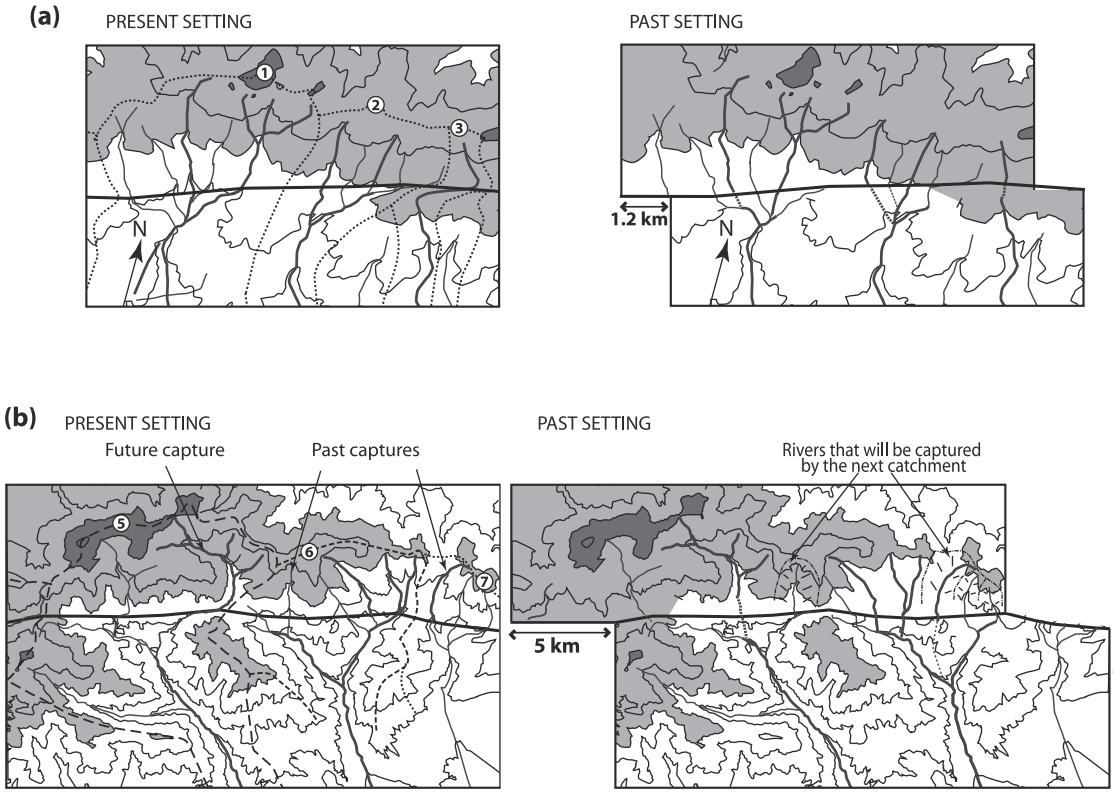

Figure 10. Drainage offset restoration in the Ilgaz Mountains (see Figure 9b for the location of the numbered catchments). (a) The wrenched shape of a series of small catchments (left) is restored to a more symmetrical initial shape by 1.2 km slip along the fault (right). (b) Larger wrenched drainage (left) require 5 km slip along the fault (right) to cancel their apparent offset. Some stream channels placed upstream of the fault provide examples of possible past and future captures.

esis is supported by two main observations. First, eroded fluvial deposits overhang the Havza-Lakik basin on its southern rim [*Barka and Hancock*, 1984; *Barka and Gülen*, 1988]. They cannot have been deposited by the small tributary flowing from Havza to Amasya, but by larger rivers, like the Yesilirmak or Kelkit, that, in our interpretation, were initially flowing through the Havza-Ladik basin (Figure 5b). Second, the present Havza river valley rises in the Ladik Lake where the fault makes a small step. It is surrounded by the larger Havza-Ladik basin filled by lacustrine sediments that have been deposited before the river capture in a larger pull-apart lake. At the time of the river capture, the water supply would have decreased, the lake recessed and the sediment deposit ended (Figure 5b). The 20 ± 5 km offset of the Havza-Ladik basin [*Barka and Hancock*, 1984] postdates the river capture and may be correlated with a similar offset of the present Yesilirmak river course (Figure 5b). We conclude that the total offset of the Yesirilmak valley is more likely about 75 km, the distance between the Havza valley and the Yesilirmak valley north of the NAF. This is a lower bound of the total NAF offset, because slip also have occurred in the pull-apart and along the Esencay fault.

3.2.3. The Kizilirmak river

[25] The Kizilirmak river is located south of the Ilgaz Mountains, about 80 km northwest of the Yesilirmak river (Figure 6a). At its confluence with the Devres river, it has a wrenched shape that corresponds to a 30-km offset. Contrary to earlier suggestions [*Barka and Hancock*, 1984; *Barka*, 1992], and as discussed in section 3.1, we do not consider that this offset corresponds to the NAF total displacement. We find it more likely that the original course of the Kizilirmak flowed along the courses now occupied by tributaries in the Vezirköprü basin, suggesting an offset of about 80 km or greater (see also section 3.1.2).

3.2.4. The Gerede river

[26] The Gerede river is located in the western Turkey between 32° and 34°E, 80 km west of the Kizilirmak river (Figure 2b). Its valley has a pronounced wrenched shape (Figure 7). In its headwater area, it flows northward into a small sedimentary basin located south of Gerede. Leaving its source region, it then flows eastward for 95 km. In the first 25 km, the river valley is located 2 to 3 km south of the fault. It then moves north and flows along the fault trace for a farther 65–70 km. Finally, west of the Ilgaz Mountains the river bends 90 to flow northwest toward the Black Sea. The form of the Gerede valley therefore suggests a total offset in the range 65–95 km.

[27] In summary, the four largest Turkish river valleys record a right-lateral displacement in excess of 65 km along the eastern and central parts of the fault (Table 1). The river offsets must always represent a lower bound on the NAF total offset, and the largest river valley deflection (80 ± 15 km for the Gerede river) correlates with the

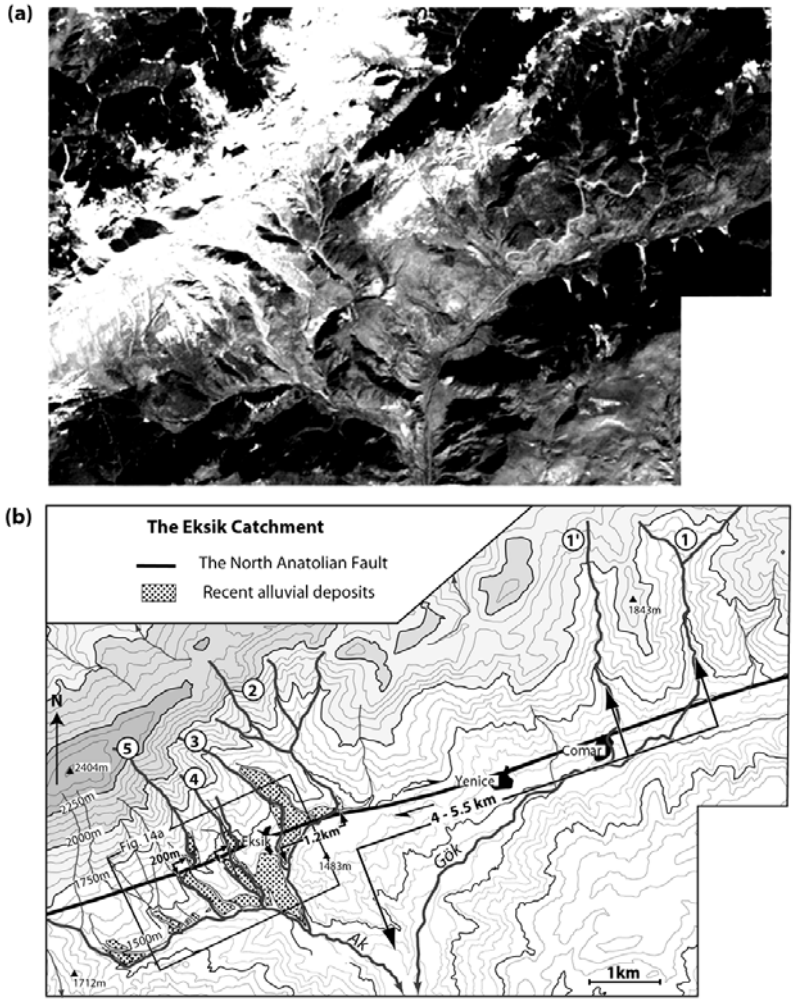

Figure 11. Drainage offsets across the NAF in the Eksik catchment (See location in Figure 6b). (a) Detail of SPOT image. (b) Corresponding map showing the offset morphology. Arrows mark valley offsets ranging from 4–5.5 km (deeply incised rivers) to 200 m (small rivers with young alluvium). The topography is from 1:25,000 scale maps (Army Geographical Service of Turkey). Rivers are numbered from 1 to 6. The location of Figure 14a is shown by a box.

structural offset of the Tosya-Vezirköprü basins (80 ± 10 km). It seems from these observations that offsets identified by earlier authors were minimum estimates that largely underestimated the actual displacement across the NAF [*Barka*, 1992]. The correct value is most probably of the order of 80 km or even greater. Moreover, the offset of the morphological markers is of the same order as the total offset (85 ± 25 km) of the Pontide suture. The later is likely to represent the total displacement of the Anatolian plate. This suggests that the NAF total offset is nearly uniform all along the fault and that most of the Anatolia/Eurasia deformation have been localized on a few kilometers on either side of the present trace of the NAF, over several million years.

4. Small River Valleys Offsets Along the NAF Bend

[28] In this section, we study the interaction between river networks and fault slip at scales varying from a few meters to a few kilometers. The observations of these scales are crucial to assess more precisely to what extent the slip is localized along the surface fault trace, and to deduce slip rates over the past 10,000 years. We use remote sensing data to map the river drainage and associated alluvium in four different regions (Gerede, main NAF bend, Erzincan, and Erbaa), which have been studied in detail. The methodology used is described more precisely for a specific area of the NAF (main NAF bend), which provides the best examples of offset morphologies at a range of scales. Similar conclusions can be drawn from the study of the three other regions, which we present in Appendix A.

4.1. Kilometric Drainage Offsets in the Ilgaz Mountains

[29] In the central part of the Ilgaz Mountains, which reach an elevation of 2587 m, the North Anatolian Fault strikes N70–80°E parallel to the crest line and cuts across seven adjacent intramountainous river catchments (Figure 9)

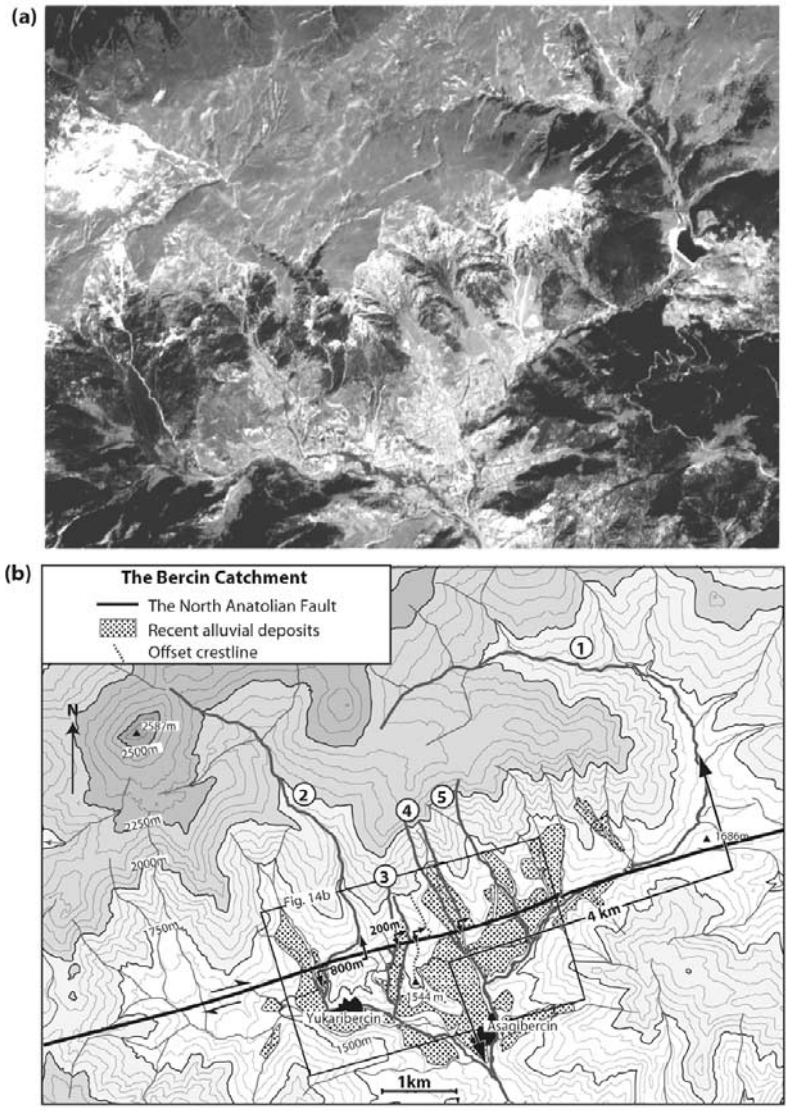

Figure 12. Drainage offsets across the NAF in the Bercin catchment (see location in Figure 6b). (a) Detail of SPOT image. (b) Corresponding morphological map showing the offset morphology. The morphology and the river valley offsets are similar to those in Eksik (Figure 11). Arrows for valley offsets (200 m, 800 m, and 4 km). The topography is as in Figure 11b. Rivers are numbered from 1 to 5. The location of Figure 14b is shown by a box.

[*Allen*, 1969; *Barka and Hancock*, 1984; *Barka*, 1992]. The drainage system, with rivers flowing SSE perpendicular to the fault strike, is disrupted at a mean elevation of 1750 m: All catchments (numbered from west to east) are twisted and elongated eastward, north of the fault (Figure 9). Their present shape results from increasing right-lateral displacement causing both valley offset (Figure 8a) and valley capture, by adjacent catchments (Figure 8b). In Figure 9b the small catchments 1, 2, and 3 have asymmetrical wrenched drainage across the fault. To restore them to a more symmetrical shape, the fault must be moved back by 1.2 km (Figure 10a). In the largest catchment 4, the distance between the easternmost river incising the basement north of the fault and the main outlet south of the fault reaches a maximum of 14 km (Figure 9b). Repeated stream captures may explain the 14-km-long elongated shape of this catchment. Farther east, catchment 5 has also a wrenched shape and its main river valley is offset by 5 km. In Figure 10b we remove 5 km of displacement along the fault to restore symmetry. As a result, other rivers align across the fault and provide examples of past stream capture.

[30] The foregoing observations indicate that rivers that have small drainage area tend to be repeatedly captured by adjacent catchments (Figure 8b) and thus do not record long-term fault motion. The detailed mechanism of how this happens is complex and depends on many factors. A major parameter, however, is the capacity of a stream to incise in order to maintain its course. This capacity, or stream power, depends monotonically on the river slope [e.g., *Julien*, 1995] as well as on the total surface of the catchment. Large catchments have a higher downstream flow and thus more stream power than smaller ones. Thus bigger rivers

can maintain their original courses longer and tend to be more offset than smaller ones. This feature is clearly observed in the Ilgaz Mountains (Figure 9b). The largest observable valley offset (14 km) occurs in the largest catchment 4 (190 km^2). Catchment 5 has a smaller drainage area of 115 km^2 and is offset by about 5 km. The other wrenched catchments 1, 2, and 3 have drainage areas smaller than 50 km^2 and are offset by about 1.2 km (Figure 10b). Over the long term, the fault motion decreases the river slope and thus the stream power [*Wallace*, 1968; *Schumm*, 1986]. Under a critical threshold the river deposits part of its bed load and fills its own channel (aggradation). Its upstream channel is then more easily captured by an adjacent river whose downstream channel is more aligned with it, promoting a higher slope and stream power. In the actively growing Ilgaz Mountains, streams are deeply incising the mountain front and stream capture should be mainly triggered by aggradation events. This aggradation/incision threshold mechanism is modulated by many other factors like climate and vegetation changes that affect the hillslope and fluvial processes [e.g., *Schumm*, 1977; *Brakenridge*, 1980; *Knox*, 1984; *Bull*, 1991]. The preexisting relief and structure in a region also affect the river channel spacing and thus the river capture process. For example, the westward elongation of catchment 4 by successive captures may be enhanced by the Tosya fold structure to the south (Figure 9b).

[31] Despite all these complexities and the fact that small rivers have limited memory, they are good markers to characterize fault activity and fault motion localization over the last hundred thousand years (for a slip rate of 20 mm/yr on the NAF, a river offset by 2 km was established 100,000 years ago). In particular, we can see that the offset of the whole morphology (rivers and associated sediments) is localized close to the trace of the NAF that corresponds to the twentieth century earthquake ruptures. This observation can be made consistently at all scales from a few meters to 14 km and strongly suggests that the continuous deformation has been localized on, or close to a single fault plane for at least a few hundred thousand years. We now illustrate this point on the two biggest wrenched catchments 4 (Eksik) and 5 (Bersin) that are offset by 14 and 5 km, respectively (Figure 9). Figures 11 and 12 show that rivers nested inside them are also deflected across the NAF trace, defining offsets at several other smaller scales. Inside the Eksik catchment, six river valleys, numbered 1–1′, 2–5, are cut by the NAF and have wrenched shapes (Figure 11). To the east, the biggest river valleys 1 and 1′ have relatively large catchments and have 300-m-deep V shapes. They are offset by 4 and 5.5 km, respectively. To the west, river valley 2 has a smaller drainage area and has also a marked v-shape. It is offset by 1.2 km. Farther west, the small stream valleys 3 to 5 have 1 to 3 km^2 drainage areas and are covered by young alluvium. They are offset by about 200 m. The Bercin catchment adjacent to Eksik has a similar morphology. It is formed by several river valleys labeled 1–4. The morphology of rivers 1, 2, 3–4 in Bercin is identical to the morphology of the rivers 1–1′, 2, 3–5 in Eksik, and their valleys are respectively offset by 4 km, 800 m, and 200 m (Figure 12). The influence of the fault may also be visible in the largest valley profile (Figure 13).

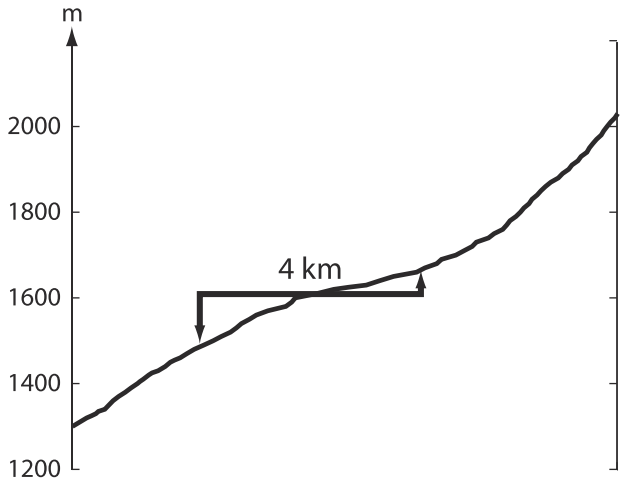

Figure 13. Longitudinal profile of the largest river valley 1 in the Bercin catchment. The profile was obtained by digitizing 1:25,000 topographic maps. The slope has a point of inflexion where the river crosses the fault and is shallower in the region where the river follows the NAF trace. The section marked 4 km indicates the approximative location of the fault.

[32] We have documented similar kilometric morphological offsets along the NAF west of the Erzincan basin and in the Gerede area. A detailed description is included in Appendix A. These drainage offsets occur along the active trace of the NAF and fit into the larger-scale offsets documented in section 3. It is important to note that no other strike-slip motion could be detected on the Spot images. All these observations, made in very different regions along the NAF (Gerede and Erzincan are separated by 650 km), show consistently that a great part of the shear strain due to the Anatolian extrusion has been localized on the active trace of the NAF for the last hundred thousand years.

4.2. The 200-m Morphological Offset in the Eksik and Bercin Catchments

[33] In Figures 14a and 14b are mapped the offset morphology in the Eksik and Bercin catchments at a fine scale, using 1:10,000 aerial photographs combined with fieldwork. In both catchments, the rivers have deeply and laterally incised the basement relief. As a result, the catchment divides form steep N-S ridges that separate 300- to 500-m-wide valleys. These valleys are filled by young alluvial sediments and end downstream into large alluvial fans. The alluvium forms a coarse, light-hued conglomerate, poorly consolidated and without clear graded bedding. The conglomerate is composed of angular pebbles/boulders with diameters in the range 5–20 cm. These young torrential deposits have similar characteristics and weathering in Eksik and Bercin.

[34] The observed ridge-and-valley morphology is offset by the NAF (Figure 14). In both the Eksik and Bercin catchments the river valleys, the ridges in between them, and the alluvial sediments infilling them, have wrenched shapes corresponding to similar 200-m offsets (Figures 15 and 16). A representative example, corresponding to the

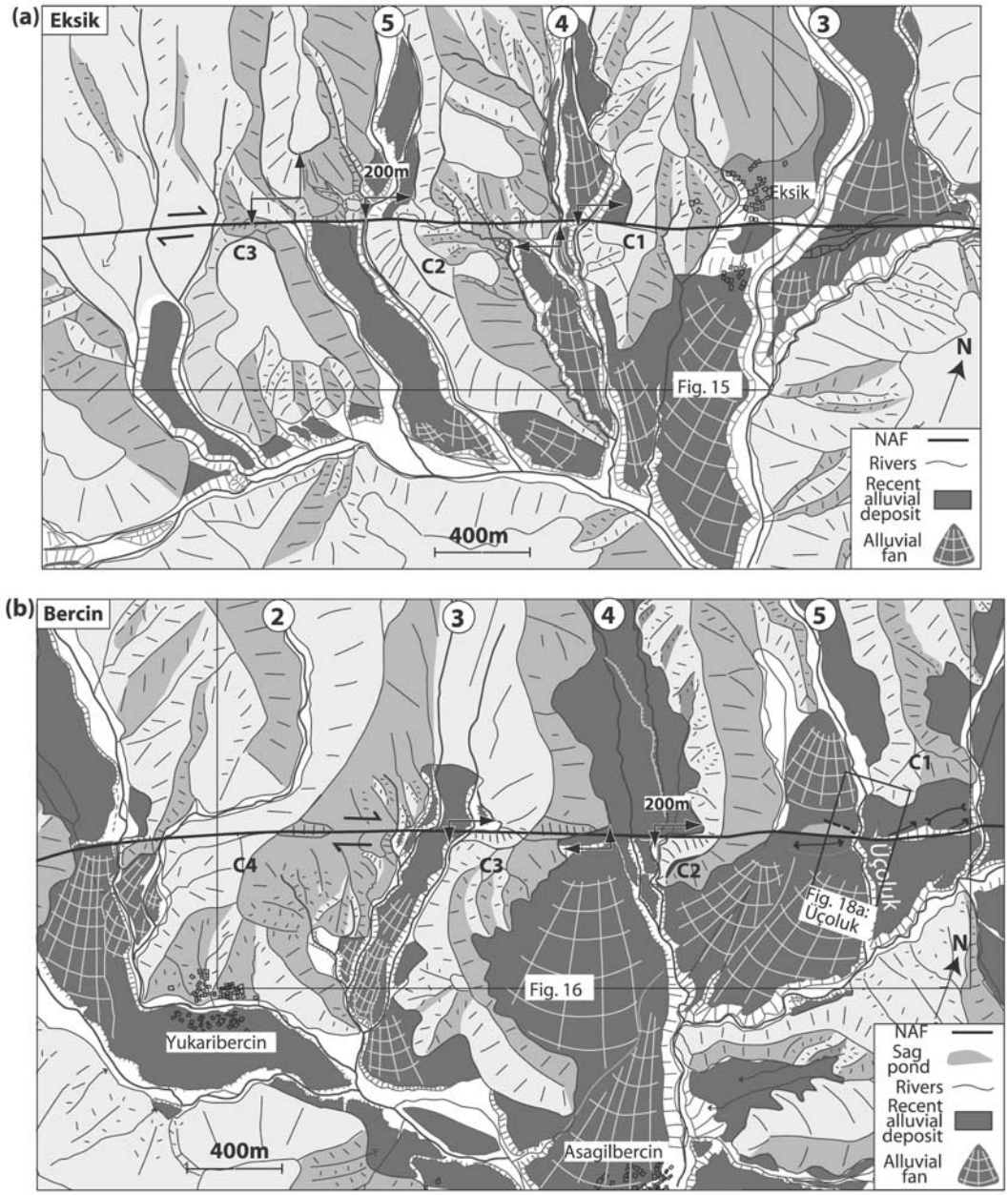

Figure 14. Detailed morphology of the NAF in the Ilgaz Mountains. (The locations of Figures 14a and 14b are shown in Figures 11b and 12b, respectively) (a) Map derived from the 1:10,000 scale aerial photographs in the Eksik area. The 200-m offsets of the ridge-and-valley morphology are marked by arrowheads. The topography has been incised prior to deposition of young alluvium in the valleys. The valleys have been subsequently offset by the slip on the fault. Figure 15 is outlined. (b) Map derived from the 1:10,000 scale aerial photographs in the Bercin area. The ridge-and-valley morphology and the 200-m offsets, marked by arrowheads, are similar to those in the Eksik area located 15 km to the west. The Üçoluk creek site (Figure 18) as well as Figure 16 are outlined.

river valley numbered 4 in the Eksik catchment (Figure 14a), is displayed in Figure 17. This valley is filled by tens of meters of young alluvium and is offset by 200 m across the NAF. Note that the two major ridges C_3 and C_4 in Bercin have wide smooth wrenched shapes that correspond to a cumulative offsets between 500 and 800 m (Figure 14b). Nevertheless, near the fault trace, the two ridges are more sharply cut and right-laterally displaced by about 200 m (Figure 16). As a result, the alluvial fan located south of the fault in the river valley 4, faces the scarp formed by the offset ridge C_3. Consequently, it is no more fed by any upstream river.

[35] To measure more precisely the offset and its homogeneity, we have restored a continuous morphology across

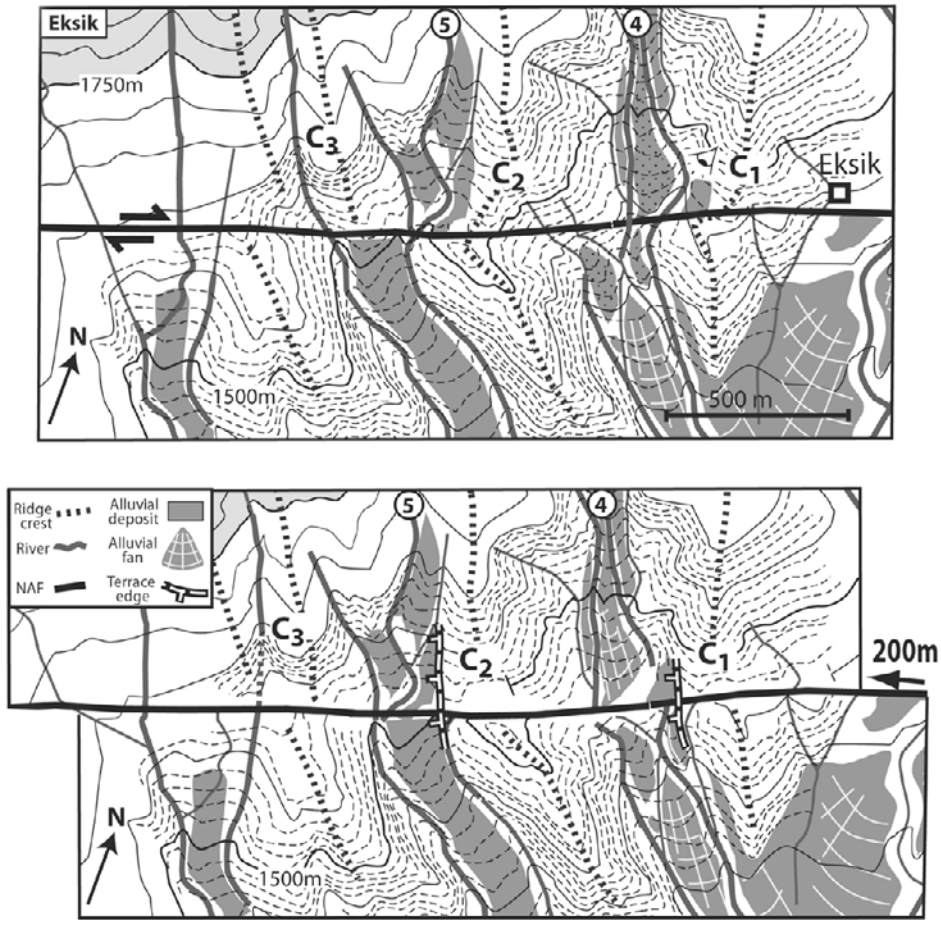

Figure 15. Drainage offset restoration for Eksik (see location in Figure 14a). (top) Present stage. (bottom) An offset of 200 m is restored, which removes the right-lateral offsets of valleys, sediments and ridges. The topography used has contour intervals of 10 m. For clarity, some contours near the fault were erased in Figure 15, bottom.

the NAF in Eksik and Bercin (Figures 15 and 16). On these maps, the ridges are well-defined markers whose shapes are constrained by several topographic contours. All along the fault we can match the steep hillslopes and narrow crests of the different ridges with the help of a homogeneous left-lateral offset of 200 m. The ridges C_1 in Eksik and C_3 in Bercin form the sharpest and the best defined relief. Their offsets can be confidently bracketed between 180 and 215 m. In the restoration of the Eksik catchment, the river valleys 4 and 5 are also aligned across the fault (Figure 15). For the Bercin catchment, in addition to the restored continuity of the ridges C_2, C_3, and C_4, the anticlinal warping in the river valley 5 is aligned with an other anticlinal form south of the ridge C_1. The upstream valley 4 also nicely extends after the restoration into an alluvial fan downstream. Similar morphological features, offset by 180 to 200 m, are found in other distant regions (Erzincan, Gerede, and Destek), as described in Appendix A.

[36] The recurrent appearance of a 200-m offset along the fault, consistently over several hundred kilometers, is a feature that deserves further discussion. The observed morphology appears to result from an incision event of the river network (river degradation) that in some cases is followed by the deposition of alluvium (river aggradation). The timescale for the formation of these structures must have been much shorter than the timescale characterizing the fault motion, as suggested by the fact that it is possible to restore precisely a continuous morphology (Figures 15, 16, A4, A6, and A8). The homogeneity of the 200-m offset is in sharp contrast with the variety of the drainage offsets documented in section 4.1. In particular, the 200-m offset seems to be independent of the catchments areas. These observations suggest that the aggradation/incision event may have been triggered by an abrupt climate change independent of individual fluvial systems. The most recent, and best known major climatic change, likely to have a major morphological impact, is that associated with the last deglaciation.

[37] Between 10,000 and 12,000 years ago, major changes in climate, sea level, and vegetation occurred in the Mediterranean area. The mean temperature in winter and summer rose by 5–10°C and 1–13°C, respectively [*Lautenschlager and Herterich*, 1990; *Harrison et al.*, 1992]. The sea level of the Mediterranean and the Black Sea increased by 110 to 120 m [*Lambeck*, 1995]. The freshwater "Black Sea Lake" became saline about 9500 years ago

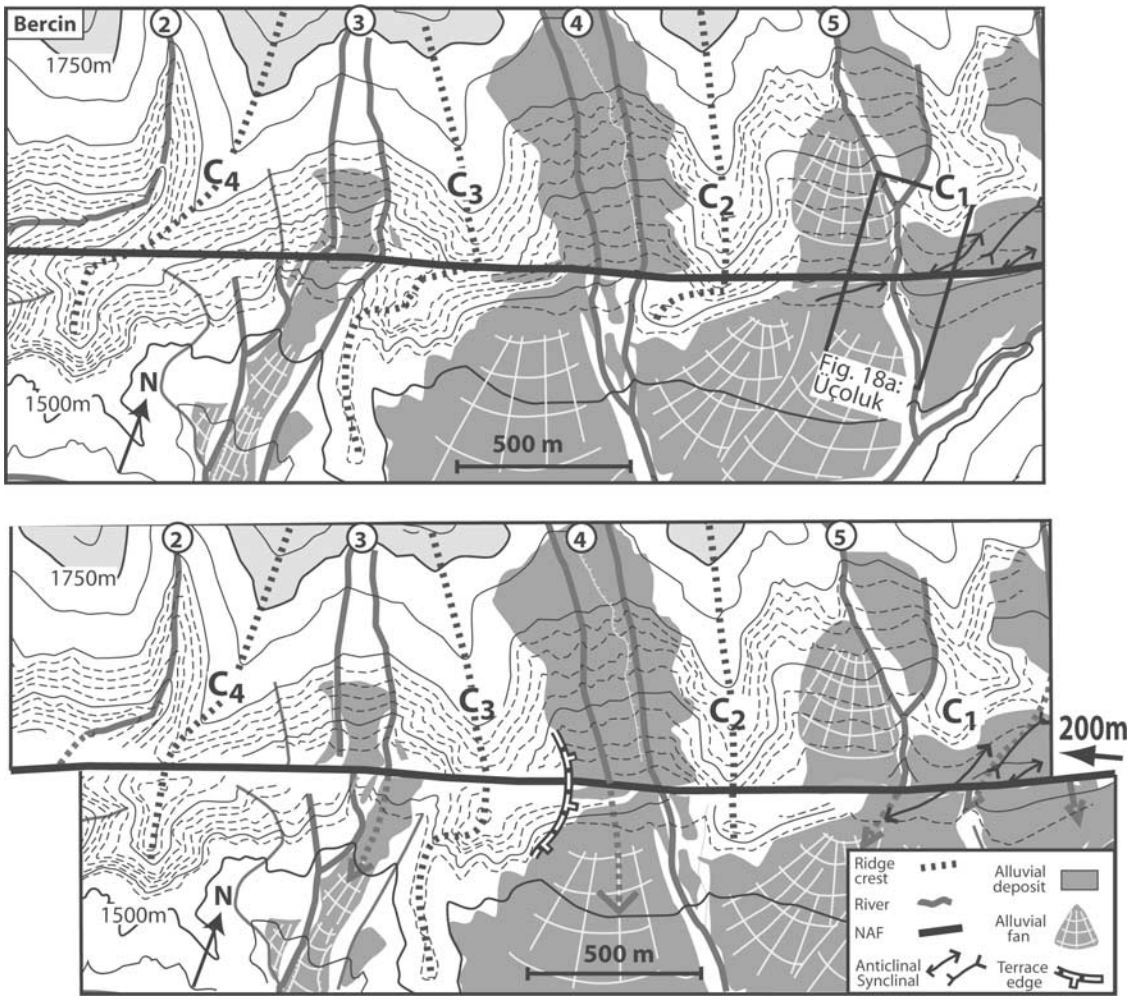

Figure 16. Drainage offset restoration for Bercin (see location in Figure 14b). (top) Present stage. (bottom) An offset of 200 m is restored, which removes the right-lateral offsets of valleys, sediments and ridges, except for C_3 and C_4 which show larger offsets. The topography and contours are as in Figure 15.

[*Stanley and Blanpied*, 1980]. The glacial period was arid with sparse vegetation and a high level of lakes. This has been interpreted as resulting from a greater seasonality during this period. During cold wet winters, water would fall mainly as snow, and during summer, drought would prevail. Both processes favor river runoff with little infiltration and evaporation of the transported water [*Prentice et al.*, 1992; *Landmann et al.*, 1996]. During the deglaciation the level of most lakes dropped drastically [*Degens and Kurtman*, 1978; *Erinc*, 1978; *Roberts*, 1983; *Prentice et al.*, 1992; *Roberts and Wright*, 1993; *Landmann et al.*, 1996] and the vegetation cover changed from an arid or semiarid steppe-tundra to an oak forest [*Bottema*, 1978; *Brice*, 1978; *Erol*, 1978; *Roberts*, 1983; *Landmann et al.*, 1996].

[38] The fluvial system response to these external perturbations could be as follows. During the glacial period, most of the rivers flowed only during springtime in mountain areas. With the decrease in seasonality during the Holocene, they became perennial and their monthly discharge increased. As a result, rivers incised and their stream bed load increased. Over the long term, the decrease in seasonality favors soil development, water infiltration and vegetation growth. These mechanisms in turn tended to decrease the stream discharge. This process can trigger valley aggradation. Rapid down cutting followed by stabilization are conditions compatible with creating and preserving the morphological features now observed to be offset by 200 m.

[39] This scenario suggests that the 200 ± 20 m offset morphology observed nowadays can be estimated to have occurred in the last 10,000–12,000 years. This gives a mean slip rate along the NAF of 18.5 ± 3.5 mm/yr over this time period. These climatic arguments are always open to discussion. However, the most recent GPS data [*McClusky et al.*, 2000] confirm that all these arguments must be right.

4.3. Slip Rate Deduced From Stream Channel Offset

[40] In this section, we further constrain the fault slip rate. The strategy is the same as in section 4.2 but applied at a smaller scale to characterize the offset of single streams and the associated alluvium. We have studied the Üçoluk creek, located in the river valley 5 of the Bercin catchment (Figure 16). It displays a clear offset morphology that is datable directly using ^{14}C.

[41] The Üçoluk stream has entrenched by several meters two alluvial surfaces that we label t_1 and t_2 (Figure 18a).

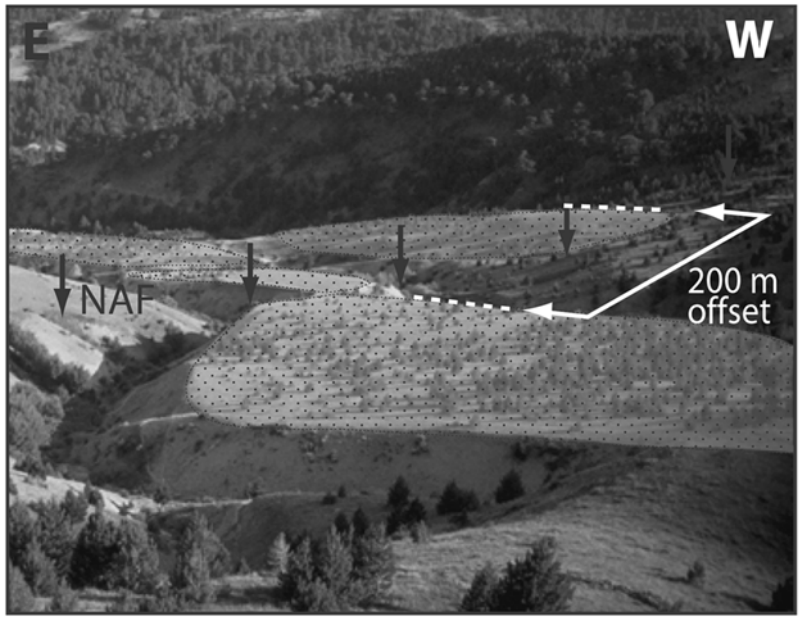

Figure 17. Photograph of river valley 4 in the Eksik catchment. This valley is filled by tens of meters of young alluvium (marked by dots). The NAF trace is marked by black arrows, and the 200-m offset across the NAF is indicated by white dashed lines.

The main surface t_1 corresponds to the uppermost surface of alluvial fans that have filled the river valleys (as mapped in Figures 14b and 16). The terrace t_1 appears to be a fill terrace (for a definition of this terms, see *Bull* [1991]). Its surface is deformed near the fault on both sides of the river. To the west of the river, the south side of the fault is upwarped and it is downwarped to the north, indicated as a sag pond. To the east, en echelon folds are cut by the fault and form a 5-m-high south facing scarp visible in topographic profiles (Figure 19a). The second alluvial terrace t_2 is nested into t_1 and preserved only on the eastern bank of the creek north of the fault (Figures 18a and 18c). This inset fill terrace forms a 125-m-long and 10–20 m wide band along the river bank. At the level of profile p_4, it is about 2.5 m below the terrace t_1 (profile p_5) and 4 m above the present-day stream channel (profile p_3) (Figures 18a, 18b, 19a, and 19b). The Üçoluk creek is bounded by the t_1 and t_2 terrace risers. These terrace risers appear to be fresh and well preserved and thus can be characterized very accurately by the profiles p_1, p_1' and p_2. The potential errors in their horizontal positions are less than 0.5 m (Figures 18a and 18b). The main feature is that two different offsets (Δ_1 = 34 m and Δ_2 = 21.5 m) are visible (Figure 20).

[42] A possible history for the formation of the above structure that is consistent with the observed morphology can be given. We first make the reasonable assumption that the relatively short incision events occur when the incision is much larger than the fault slip rate. This implies that the terrace risers should cross the fault without visible offset just after their formation, and is consistent with the fact that we are able to restore a continuous morphology after suitable left-lateral offsets (Figure 20). As t_1 is a fill terrace, its offset dates from the time the alluvial fan was incised by the stream some τ_1 years ago (Figure 20). The nested terrace t_2 was deposited later, and subsequently incised τ_2 years ago (Figure 20). The two different offsets Δ_1 and Δ_2 observed on the morphology correspond to the two episodes of incision, dated by τ_1 and τ_2. As shown in Figure 20, a left-lateral slip of 21.5 ± 1 m restores the continuity of the t_2 riser and the present river channel, and an additional 12.5 ± 2.5 m left-lateral slip cancels totally the wrenched shape of the t_1 riser (Figure 20). The total 34 ± 3.5 m offset of the t_1 risers has a few meters uncertainty, because they have been partly reshaped during the incision of the terrace t_2.

[43] The ^{14}C dating of charcoal in two trenches along the t_1 and t_2 terrace risers constrain the age of the episodes of terrace formation. The sampling trench profiles in t_1 and t_2 are described in Tables 2 and 3 (see also photographs in Figure 21). We have dated two samples found in clay layers in the t_1 eastern riser, 180 m north of the fault, 1 and 1.3 m deep, and a third sample 1.35 m deep in the t_2 riser, 25 m north of the fault (Figures 18a and 21). The samples are under the first angular gravel bed that should represent the last deposits before terrace abandonment and stream incision [*Merrits and Vincent*, 1995]. The samples ages corresponding to t_1 are 4310 ± 80 years for the deeper and 3970 ± 80 years for the shallower, and thus younger, charcoal. The sample age corresponding to t_2 is 1640 ± 60 years.

[44] Since the Δ_2 = 21.5 ± 1 m offset must be younger than the formation of the terrace t_2, we deduce a minimum slip rate on the fault of 13 ± 0.5 mm/yr. This result is independent of the nature of terrace t_1. The total offset Δ_1 = 34 ± 3.5 m must be older than the formation of terrace t_2. This yield a *maximum* slip rate on the fault of 21 ± 2 mm/yr. The dates obtained in terrace t_1 are

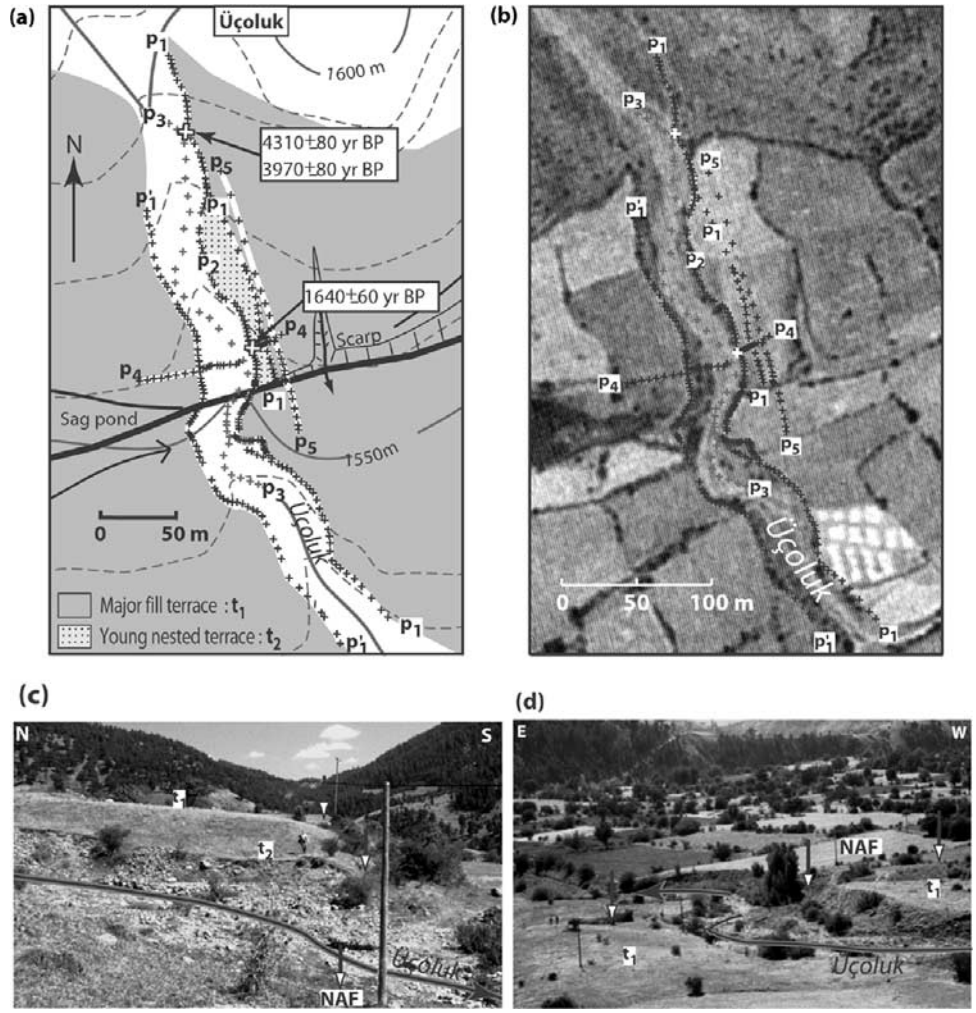

Figure 18. The Üçoluk river site (see location in Figure 14b). (a) Map of the site (the topography is the same as in Figure 16). The measurement points of six leveled topographic profiles p_1 to p_6, measured with a theodolite and distance meter Wild T 2000 and DI 3000, are indicated with black crosses. The total station is situated less than 500 m away from measured points, and thus the apparatus accuracy is centimetric. Profiles p_1, p_1', and p_2 follow the edges of the terraces t_1 and t_2; p_3 follows the bed of the river; p_5 runs at the top of the main terrace; and p_4 is parallel to the fault trace and crosses the other profiles at a right angle. Two trenches dating terraces t_1 and t_2 are marked by white crosses. The charcoals sampled in the two trenches were dated at the accelerator mass spectrometer at Gif-sur-Yvette (France) and calibrated for ^{14}C production changes under the supervision of F. Grasse. (b) Aerial view corresponding to the map in Figure 18a. Bold arrows indicate the trace of the NAF. Location of trenches and measurement points of profiles as in Figure 18a. (c) The two terrace risers t_1 and t_2 upstream from the fault trace are visible on the eastern bank of the Üçoluk river (view from the west). The fault is indicated by arrows, and the position of the current active stream channel is indicated by a solid black line. (d) The right-lateral offset in the Üçoluk creek (view from the north). Fault and stream are as in Figure 18.

consistent with the preceding results, but do not constrain further the slip rate. The foregoing study of the Üçoluk creek allows us to bracket the slip rate of the NAF during the last few thousand years between 12.5 and 23 mm/yr. Most of the shear strain appears to be concentrated on the present NAF trace over this time period.

5. Discussion and Conclusion

[45] Our observations have focused on offset structures at a range of scales from a few meters up to 90 km along the NAF. From the study of the Üçoluk creek, which displays an offset morphology of 21.5 ± 1 m to 34 ± 3.5 m, we deduced an average slip rate of 18 ± 5 mm/yr over the last few thousand years using ^{14}C dating. We have interpreted the recurrent appearance of 200 ± 20 m morphological offsets over several hundred of kilometers along the fault as being related to the major climatic change associated with the Holocene deglaciation. This gives an average slip rate of 18.5 ± 3.5 mm/yr over the last 10,000–12,000 years. These results are consistent with the NAF seismic deformation rate which ranges between 10 and 30 mm/yr [*Jackson and*

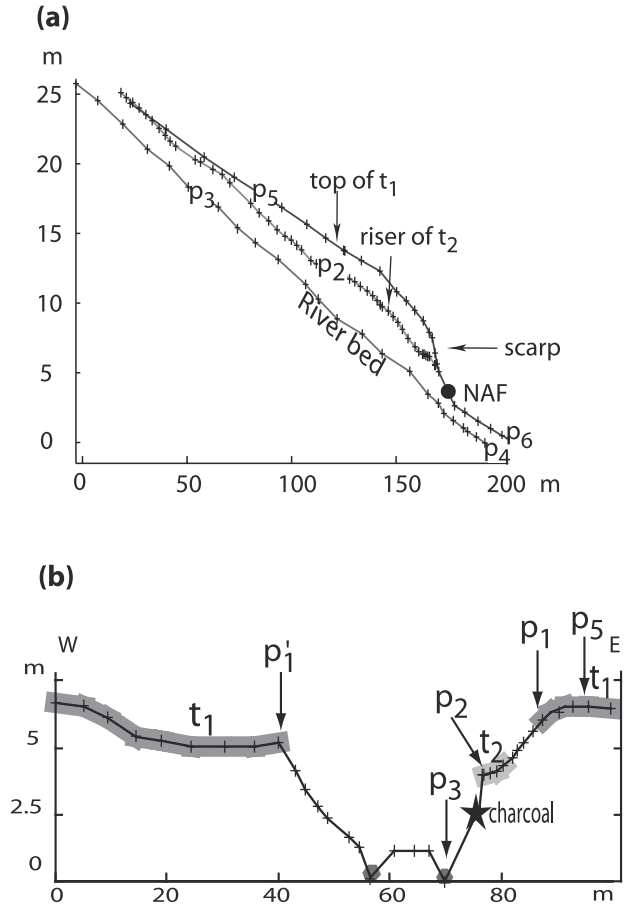

Figure 19. Profiles in Üçoluk creek site (see locations in Figure 18a). (a) Profiles p_2, p_3, and p_5 projected perpendicular to the fault. Measurement points are indicated with black crosses. (b) Profile p_4 across the river and the two terrace risers (t_1 and t_2). Measurement points are indicated with black crosses. A star indicates position of the dated sample in the trench across t_2.

McKenzie, 1988; *Westaway*, 1994]. This slip rate is, within the errors, the same as the rate of 22 ± 3 mm/yr monitored with GPS measurements in the last 10 years [*Straub et al.*, 1997; *McClusky et al.*, 2000].

[46] These observations are consistent with the deformation being confined to the immediate region of the fault. We estimate that deformation are concentrated in about 10 m for the Holocene offsets, in about 100 m for kilometric offsets of small river valleys and in about 1 km for 65–90 km offsets of large rivers and geological structures. All these offsets are closely related with the fault and specifically with the fault that moved in twentieth century earthquakes, suggesting that localization of deformation appears to have persisted for million years. No significant deformation extends over a wider region except where the fault bends or steps as in the Erzincan and Erbaa pull-apart basins or in the Ilgaz Mountains (main fault bend). The same conclusions have been obtained from a study of the western part of the NAF, in the Marmara Sea area [*Armijo et al.*, 1999].

[47] Independent of our evaluation of the slip rate on the NAF, we have also been able to constrain the total offset on the fault in its eastern and central part, by analyzing the offsets of the largest river valleys and the Tosya-Vezirköprü basins. Although of limited resolution, there is no evidence of these river valleys being offset except where they cross the fault. The 80 ± 15 km measured total offset on the fault in its eastern and central part is the same as the total offset of the Pontide suture 85 ± 25 km (Table 1). The total deformation between Anatolia and Eurasia thus appears to have been accommodated along the NAF, consistent with the earlier arguments based on slip rates.

[48] Since all the deformation seems to be closely related to the surface expression of the fault, for all time periods, it seems unlikely that it is a superficial feature and thus probably extends below the seismogenic depth. The GPS data only concern a 10 year period, but clearly exclude distributed deformation in the lower crust over that time period. Thus models that assume a viscous rheology for the continental lithosphere, with deformation distributed over hundreds to thousands of kilometers below the seismogenic depth [e.g., *Molnar et al.*, 1999], are not correct in Anatolia. This view is further supported in a second paper [*Hubert-Ferrari et al.*, 2002], which shows that a consistent picture of the NAF propagation over the long term can be explained if the lithosphere has an elastoplastic rheology. In this model, we can reconcile the facts that (1) the NAF total offsets are the same in east and west, (2) the present slip rate is uniform along the NAF, and (3) the NAF age is 13 Ma in the east and 5 Ma in the west. The NAF behavior can be modeled using elastic fracture mechanics, with a faster slip in the process zone at the tip of the propagating fault to catch up to the same total offset.

[49] While the NAF seems to have always been in the same place with deformation restricted to a narrow zone, the rate appears to have changed. If movement on the NAF initiated 13 Myr ago, shortly after the beginning of the Arabia/Eurasia collision, then the long-term slip rate would be 6.5 mm/yr. This is one third of the more recent rate. Three possible explanations can be reviewed:

1. Deformation was distributed in the earlier period and has only become localized more recently. This possibility seems to be precluded by the evidence for strike-slip deformation being closely restricted to the fault zone and the absence of significant strike-slip deformation in the Pontides. If the fault rate had remained constant at around 20 mm/yr for the whole period other structures would have had to accommodate twice as much deformation as the NAF. Such deformation would be observable.

2. Deformation has always been localized, but the age of the onset of faulting is overestimated at its eastern end. Thus a constant slip rate is possible if the fault initiated 4 to 5 Mry ago, 10 to 11 Myr after the beginning of the Arabia-Eurasia collision (15 Ma). This would imply that the fault initiated simultaneously at its eastern and western ends or propagated very rapidly from east to west.

3. The deformation has remained localized on the NAF since motion started on it, but the slip rate, was much less in the past than it is now. This change of rate may have been associated with the progressive change of the plate configuration as the NAF growth. The westward propagation of the NAF toward the Hellenic trench may have lead in recent geological times to a more stable plate configura-

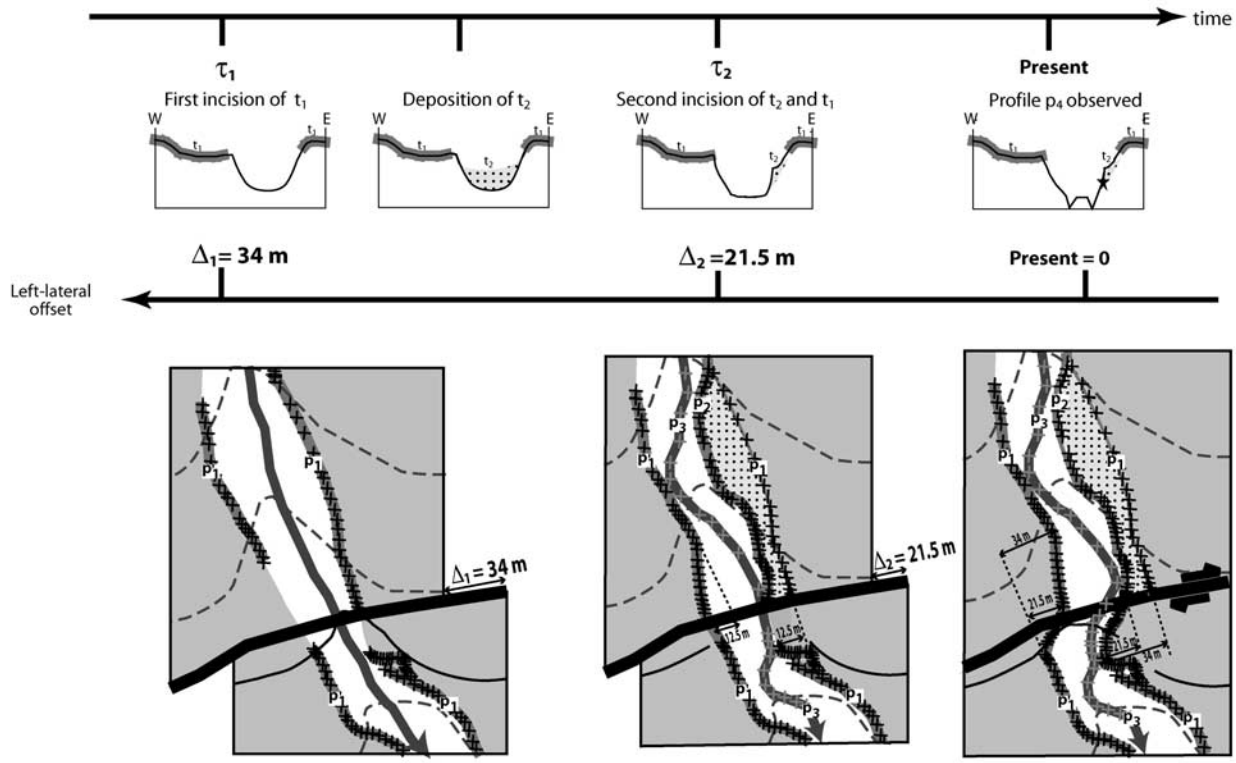

Figure 20. Formation of terraces t_1 and t_2 as fault slip increases. (top) Profile across the creek and (bottom) map. From left to right, the alluvial fan t_1 was deposited and incised by the stream some τ_1 years ago. The nested terrace t_2 was deposited later and subsequently incised τ_2 years ago. The t_1 and t_2 risers, whose shapes are constrained by the profiles p_1, p_1', and p_2 (black crosses), are offset by $\Delta_1 = 34$ m and $\Delta_2 = 21.5$ m, respectively. The age of Δ_1 and Δ_2 corresponds to the first incision event of the surface t_1, τ_1 years ago, and to the incision of the terrace t_2, τ_2 years ago, respectively.

tion with the complete separation of the Anatolian-Aegean block from the rest of Eurasia.

Appendix A: Morphological Offsets Along the NAF

A1. The Erzincan Region

[50] About 450 km east of the Ilgaz Mountains, the NAF cuts across another mountain range culminating at 2749 m and located just west of the Erzincan basin (Figure 3). The intramountainous catchments crossing the NAF, whose rivers are flowing SSW into the largest Cardakeli river, have wrenched shapes (Figure A1) like in the Ilgaz Mountains (section 4.1). The major difference between the two regions is due to the fault geometry. West of Erzincan, the fault bends by more than 15 in 10 km between Mihar and Bahik (Figures A1a and A1b). In the restraining bend area the NAF surface trace forms four

Table 2. Profile of Trench in Terrace t_1

Horizon	Thickness, cm	Characteristics
A	0–25	many small angular pebbles, a few bigger(10–20 cm) low organic clay matrix with little sand (50% of volume)
B1	25–62	few small angular pebbles and very few boulders larger than 25 cm Matrix with 90% of clay (90% of volume) and low organic content
B2	62–74	many small angular pebbles (<1 or 2 cm in diameter), a very few larger; matrix with 90% of clay (25% of volume)
B3	74–90	some boulders; matrix with 90% of clay (90% of volume)
B4	90–100	boulders (10, 20, 30 cm); matrix with 90% of clay (50% of volume)
B5	100–110	fine layers consisting of pure clay; several charcoal pieces a few millimeters in size, dated at 3970 ± 80 years ago
B6–C	110–200	angular pebbles/boulders (different sizes up to 30 cm, many 10 cm and some 1 cm); clay matrix with very little sand; some layering with slightly more pebbles at some layers Numerous charcoals in a clay lens, dated at 4310 ± 80 years ago

Table 3. Profile of Trench in Terrace t_2

Horizon	Thickness, cm	Characteristics
A	0–25	small angular pebbles, a few bigger (10–20 cm); and and low organic clay matrix (50% of volume)
A–B	25–40	transition from A to B
B1	40–90	small subangular pebbles down to gravels with a few larger stones (≥20 cm in diameter); clay matrix with 25% of silt and sand (50% of volume)
B2	90–130	similar to B1 but higher proportion of angular pebbles and less clay in the matrix
B3	130–135	clay lenses with very little small pebbles; tiny fragments of charcoal in one clay lens, dated at 1640 ± 60 years ago

1-km-long, en echelon segments. Farther west, near Mihar, the N107°E striking fault trace is sharper and cuts through a 2730-m-high pass between the Cimen and Karadag Mountains. East of the bend, the N120–124°E striking NAF forms small nested pull-aparts around Bahik. North of the main fault, a 20-km-long secondary fault zone may accommodate part of the deformation induced by the restraining bend.

[51] Despite the apparent fault complexity, catchments recording cumulative fault motion and the 1939 surface breaks show similar right-lateral offsets across the bend, which attest to localized deformation at depth along a single fault plane. The 1939 earthquake is associated with 6 m slip on both sides of the fault bend (Figure 4) [*Barka*, 1996]. The largest Mihar, Misuyu, and Kalbaris catchments that are located respectively east, in and west of the fault bend, have similar 3.75, 2.3, and 2.3 km offsets, respectively (Figure A1b). Note that the easternmost rivers of the large Kalbaris and Mihar catchments appears to have been captured recently by the adjacent catchments. Figure A1c shows that the smaller catchments have also asymmetrical wrenched drainage across the fault that correspond to smaller 800 m to 1.3 km offsets. Thus, like in the Ilgaz Mountains, the greatest offset occurs in the largest catchment (section 4.1). That the fault geometry is more complex and the largest catchment area smaller (~30 km^2), may explain why the maximum offset in the region west of Erzincan (3.75 km) is smaller that in Ilgaz.

[52] In the Mihar catchment, we documented, like in Eksik and Bercin (section 4.2), some kilometer-scale to meter-scale morphological offsets along the trace of the 1939 surface rupture (Figure A2), which attests to localized deformation. The Mihar catchment is globally offset by 3.75 km: its easternmost river 7 appears to have been captured recently by the adjacent Keko valley and is still linked to the Mihar valley by an abandoned channel filled by young alluvium. The rivers and associated alluvium located west of Mihar are also deflected across the NAF, defining offsets at smaller scales. For example, the main river 3 that has deeply incised the relief, is offset by 1.2 km with respect to the catchment outlet. To the west, a small alluvial terrace is offset by about 180 m. In Figure A3, the offset morphology has been mapped in more detail using 1:10,000 aerial photographs combined with fieldwork. The fine-scale morphology is very similar to the ridge-and-valley morphology in Eksik and Bercin.

[53] In the central part of the Mihar catchment, rivers 2 and 3 have wide channels resulting from sideways erosion. These valleys are filled by young alluvial deposits composed of angular pebbles and boulders covered by a thin carbonated crust. The alluvial terrace located between rivers 2 and 3 stands 20 m above the youngest alluvium and is thus older. Higher erosional surfaces also remain along the catchment divides 2 and 3, where they are more

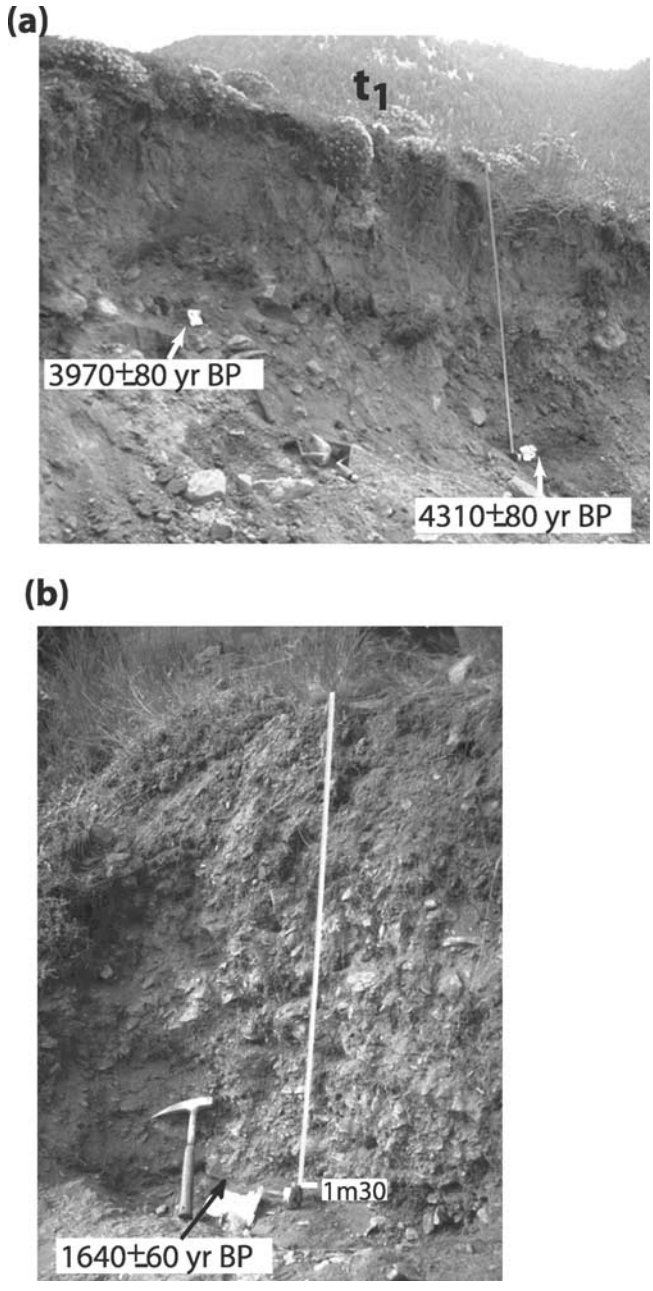

Figure 21. Sampling trenches and dates in Üçoluk creek site (see locations in Figure 18a). (a) Trench across terrace t_2. The date of charcoal sample at 1.3 m depth from t_2 surface is indicated. (b) Trench across terrace t_1. Two charcoal samples at 1 and 1.3 m depth below the t_1 surface yield consistent ^{14}C ages.

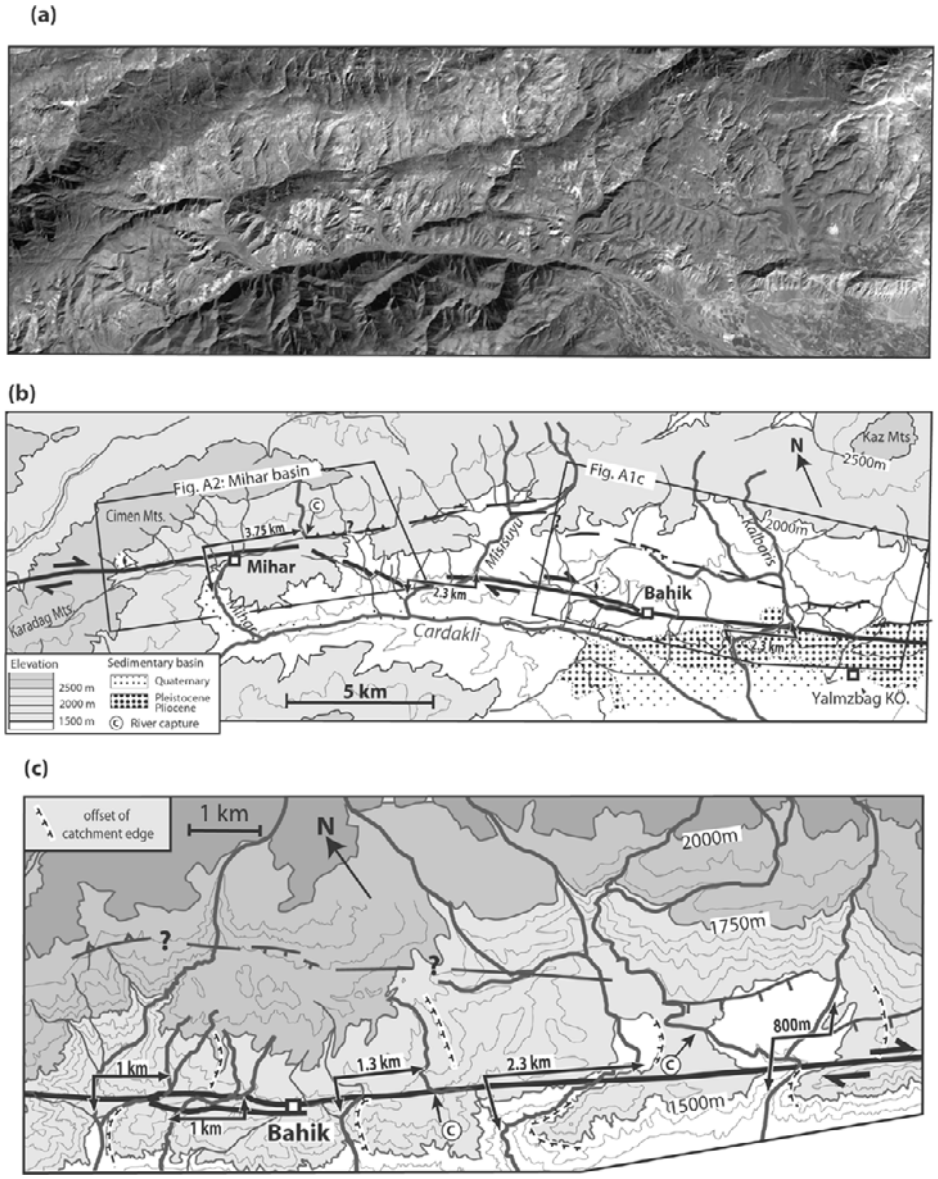

Figure A1. The NAF in the northwestern part of the Erzincan basin (see location in Figure 3). (a) Panchromatic SPOT image (10-m resolution). (b) Corresponding map showing the trace of the NAF and the offset drainage. The NAF bends more than 15 in 10 km. The largest Mihar, Misuyu, and Kalbaris catchments have similar respective 3.75-, 2.3-, and 2.3-km offsets. The topography is from 1:100,000 scale maps (Army Geographical Service of Turkey). The viewpoints for photographs showing the 6-m slip of the 1939 rupture (Figure 4) are indicated by ''photo.'' Frames for the location of Figures A1c and A2 are shown. (c) Details of drainage offsets near Bahik (topography from 1:25,000 scale maps).

protected against fluvial erosion. These surfaces join upstream with the mountain front. These old erosional surfaces are deeply incised downstream along rivers 4 and 5, which have narrow, 30-m-deep channels. The incision and lateral erosion associated with rivers 2 and 3 have been more important, so their valleys are larger and covered by recent alluvium, and the remnant outcrops of the old erosional surfaces are smaller. The incised morphology in Mihar is right-laterally offset across the NAF. The young alluvium deposited in the wide river valley 3 has a wrenched shape corresponding to a 150-m offset. To the west, the higher terrace is offset by 170–180 m. To the east, shutter ridges deviating rivers 4 and 5 downstream of the fault, result from a 200–220 m offset of the old erosional surfaces. River valley 4 is apparently offset 390 m. These various offsets can be combined to obtain an average 185 ± 35 m displacement of the incised morphology without taking into account the 390-m offset that must be older.

[54] To test the coherence of this average offset, a 185-m right-lateral displacement is restored along the fault (Figure A4). In Figure A4 the high terrace between rivers 2 and 3 and the old erosion surfaces are continuous across the fault, and the wrenched shape of the river

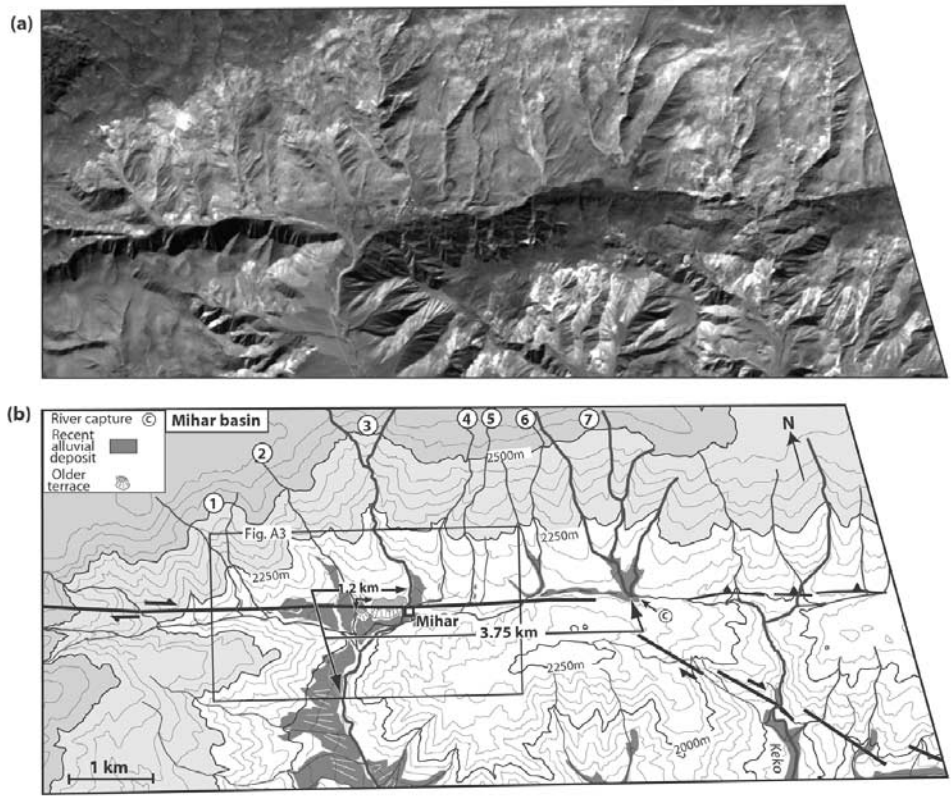

Figure A2. The NAF in the Mihar valley (see location in Figure A1). (a) Detail of SPOT image. (b) Corresponding morphological map. Possible offsets of Mihar valley range between 1.2 and 3.75 km. The larger offset corresponds to a valley that has been probably captured recently by the next river draining to the southeast (river Keko). Compare with evolution in Figure 8. Alluvial sediments deposited prior to the river capture fill the gap between the Mihar river and the point of capture (circled c). Rivers are numbered from 1 to 7 and are referred to the text and Figure A3. Topography at 1:25,000 scale.

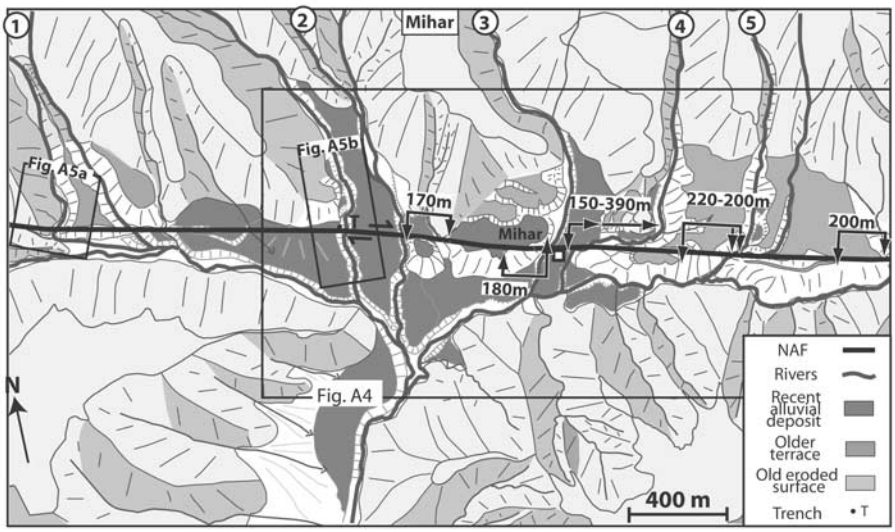

Figure A3. Detailed morphology of the NAF near Mihar (See location in Figure A2). Map derived from the 1:10,000 scale aerial photographs. Streams are numbered as in Figure A2b. Channels of streams 4 and 5 are deeply incised in a high erosion surface and appear to be offset by 200–220 m. Risers carved in a lower alluvial terrace between streams 2 and 3 are offset by 170–180 m. A riser in still lower (thus more recent) alluvium of river 3 is offset by 150 m. Frames for the locations of Figures A4 and A5 are shown.

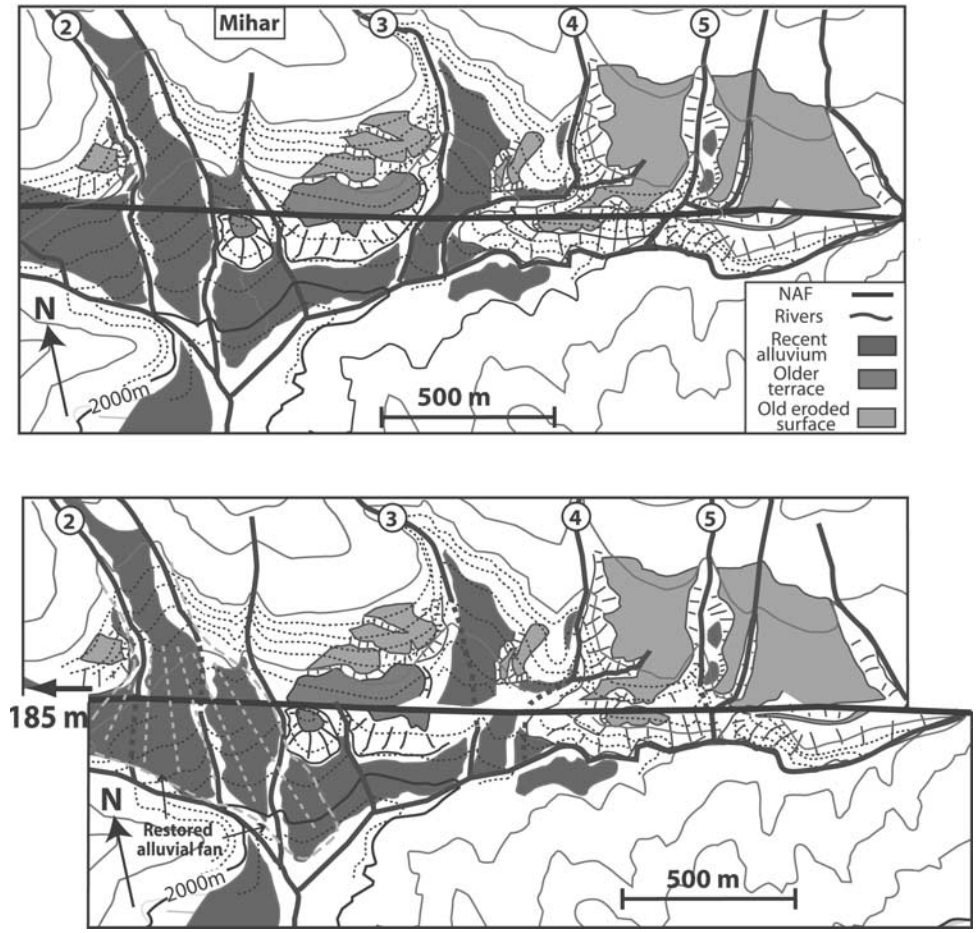

Figure A4. Drainage offset restoration in Mihar (see location in Figure A3). (top) Prresent stage. (bottom) An offset of 185 m is restored, which removes the right-lateral offsets of old eroded surfaces along river valleys 4 and 5 and of a younger terrace located between river valley 1 and 2. Features are represented as in Figure 15.

valley 3 is cancelled. To the west, alluvium in valley 2 forms a continuous alluvial fan across the fault. Young alluvial deposits in the offset valley 3 around Mihar should have been deposited latter, since they are not continuous across the fault. The restoration suggests that the incised morphology is coherently offset by 185 ± 35 m along the fault, an amount similar to the ridge-and-valley offsets documented in the Eksik and Bercin catchments.

[55] Smaller right-lateral offsets similar to the Üçoluk creek offset (section 4.3) can also be documented in the Mihar catchment. Rivers have reincised by 5 to 10 m the youngest alluvial deposits and offsets measuring tens of meters are observed across small creeks (Figure A5). For example, analysis of aerial photographs combined with fieldwork along river valley 1 shows that a shutter ridge deviates there the stream valley by 32 m, and that the riser of a small inset terrace on the east bank of the stream is offset by 15 m (Figure A5a). To the east, topographic profiles can be used to characterize a similar offset in the river valley 2. Figure A5b shows that the fan surface labeled t_1 has been incised and that well-defined risers 10 m higher than the present stream borders the stream. A younger terrace t_2 is nested on the western bank of stream, north of the fault. Three topographic profiles leveled along the risers of the main terrace t_1 and along the river bed constrain the offset of t1 risers between 19–26 m on the eastern bank and 28 m on the western bank. Offset of the eastern riser is smaller than the western one as the river flow continuously erodes it. These offsets could correspond to cumulative slip of 4 earthquakes having a 6–7 m displacement similar to the 1939 earthquake. Unfortunately, it was not possible to date these terraces because we did not find charcoal layers in the few trenches we dug.

A2. Drainage Offsets in Destek

[56] West of the Erbaa pull-apart located midway between the Ilgaz Mountains and the Erzincan basin, the NAF near Destek cuts through a small 1050-m-high relief and offsets nine catchments at a mean elevation of 650–

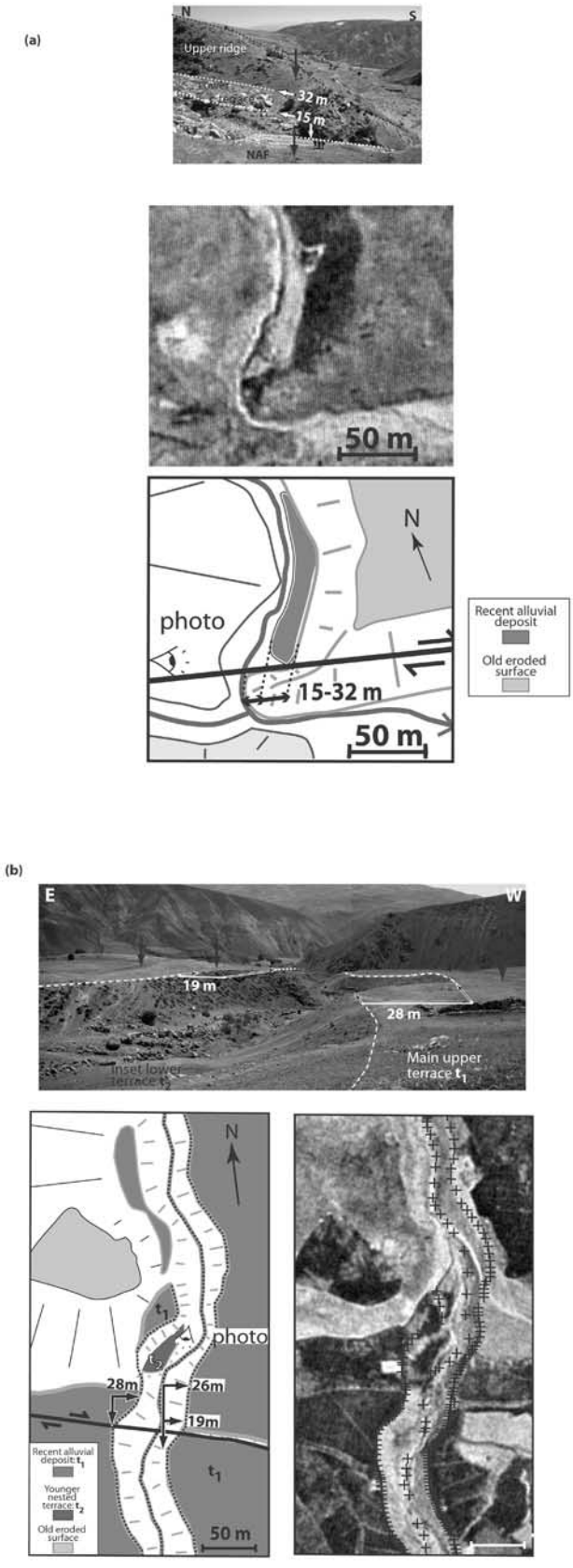

850 m (Figures 5a and A6). Using 1:25,000 scale topographic maps and a SPOT image, the drainage and the associated alluvium can be mapped in detail. The main rivers have incised the relief forming distinct small valleys. Some of the latter have been filled downstream by young alluvium (see valleys 2, 4, 5, 7, 9, and 10 in Figure A6b). The catchment divides form wide spurs to the north of the fault and more rounded hills to the south. They are closely spaced by about 500–1000 m, which implies that no kilometric offset can be documented. Aerial photographs were not available in this area and thus the morphology could not be mapped in greater details.

[57] All river valleys are offset along the fault. Using the 1:25,000 topographic maps, valley offsets have been measured with a precision of about ±25 m (±1 mm on the map). The offsets of the valley edges were reported on Figure A6b with the corresponding offset measurements reported below. Most measurements were done on the eastern edges of valleys, where the development of shutter ridges downstream of the fault preserves upstream reaches from erosion. The eleven offset measurements vary between 125 and 250 m with a average of 200 m. For example, river valley 4, that is covered by sediments, has a wrenched shape corresponding to a 250 ± 25 m offset. River valley 5 forms a double bayonet and its offset ranges between 145 and 225 m. River valley 8 is filled by alluvium and its eastern edge is offset by 190 m. Valley offsets seem to have a great variability. To test the validity of the average offset value obtained, we restored 200 m slip along the fault (Figures A6b and A6c). As a result, valleys and the associated alluvium cross the fault with almost no visible offset, river courses are straighter, and catchments are more symmetric than the present ones (Figure A6c). For example, the wrenched shapes of river valleys 1, 2, 4, 5, 6, 7, and 9 are cancelled and sediment deposits associated with rivers 4, 8, and 9 are continuous across the fault (Figure A6c). Spurs, that separate catchments 3 to 9 north of the fault, are aligned with the rounded catchment divides south of the fault. The present river valley 3 has no apparent offset but could result from a recent capture; in the restored figure it would flow in an adjacent abandoned channel covered by alluvium, downstream the fault. The fine morphology in this area flatter than the mountain areas of Ilgaz and Erzincan, is also characterized by incised valleys coherently offset by about 200 m. The apparent greater variability of measured offsets cannot be characterize furthermore due to the lack of accuracy of the available maps in this area.

A3. Drainage Offsets in Gerede

[58] About 200 km west of the Ilgaz Mountains, the NAF striking N77°E cuts through a small 1911-m-high mountain

Figure A5. (opposite) Small drainage offsets in Mihar (see locations in Figure A3). (a) (top) Photograph, (middle) aerial view, and (bottom) interpretation of a young nested terrace offset (15–32 m). (b) (top) Photograph, (bottom right) aerial view, and (bottom left) interpretation of alluvial fan risers offset by 19–26 m.

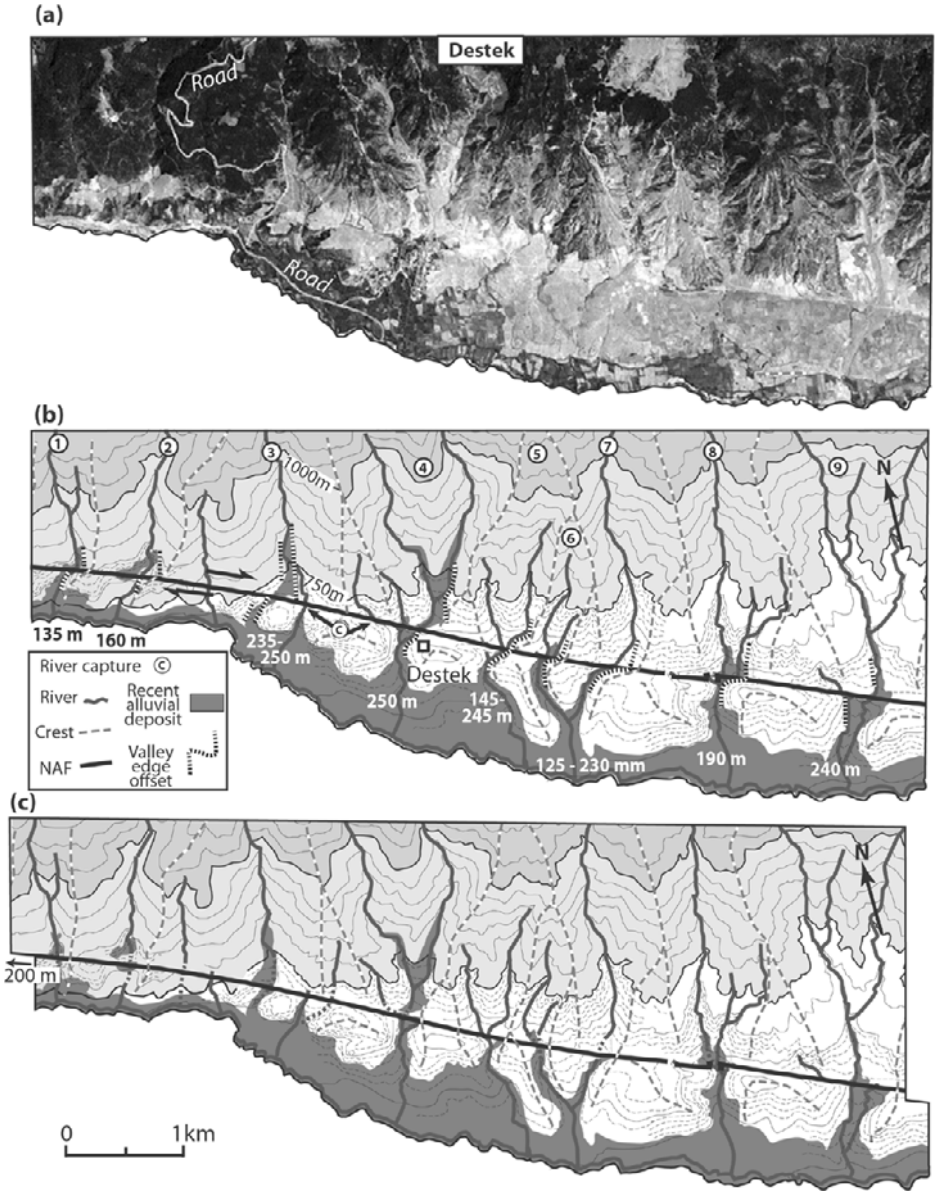

Figure A6. Drainage offsets in Destek, west of the Erbaa pull-apart (see locations in Figure 5a). (a) SPOT image. The southern border is the main river flowing eastward. (b) Corresponding morphological map (1:25,000 scale topography). Apparent right-lateral valley offsets range from 125 to 250 m (offset values are written below). The error in offset estimates is about 25 m. Circled c indicates two streams that may have been beheaded, then captured by next downstream valleys. Rivers are numbered from 1 to 9. (c) The river valley system can be restored by 200 m slip.

range and deflects right-laterally four main adjacent catchments. The catchments 2, 3, and 4 have westward elongated shapes and the distance between their easternmost rivers incising the relief north of the fault and the main outlets south of the fault reaches maxima of 2.5, 2.2 (Figure A7), and 6 km (not visible, to the east of Figure A7), respectively. The morphology in this region appears to be different than that in Ilgaz, Erzincan, or Destek. Figure A7 shows that the relief is nearly flat near the fault since the slope of the relief decreases abruptly about 300 m north of the NAF. The fault depression is filled by numerous alluvial fans and older higher alluvial terraces. Downstream the fault, shutter ridges standing 50 m above the present streams deviate the river drainage and are crossed locally by the largest rivers that have kilometric offsets. In Figure A7b the largest Kazlar, Nur, Kizilkaya, Kazan, Koy, and Canglankaya rivers have deeply incised valleys north of the fault and define 650 m, 1.1 km, 1.1 km, 600 m, 2.2 km, and 1 km offsets with respect to their outlets downstream.

[59] Analyzing 1:10,000 scale aerial photographs, the fine offset morphology between the Nur river in catchment 1 and the Kizilkaya river in catchment 2 can be characterized in details (Figures A7 and A8) and compared to the one documented farther east along the fault. In the aerial

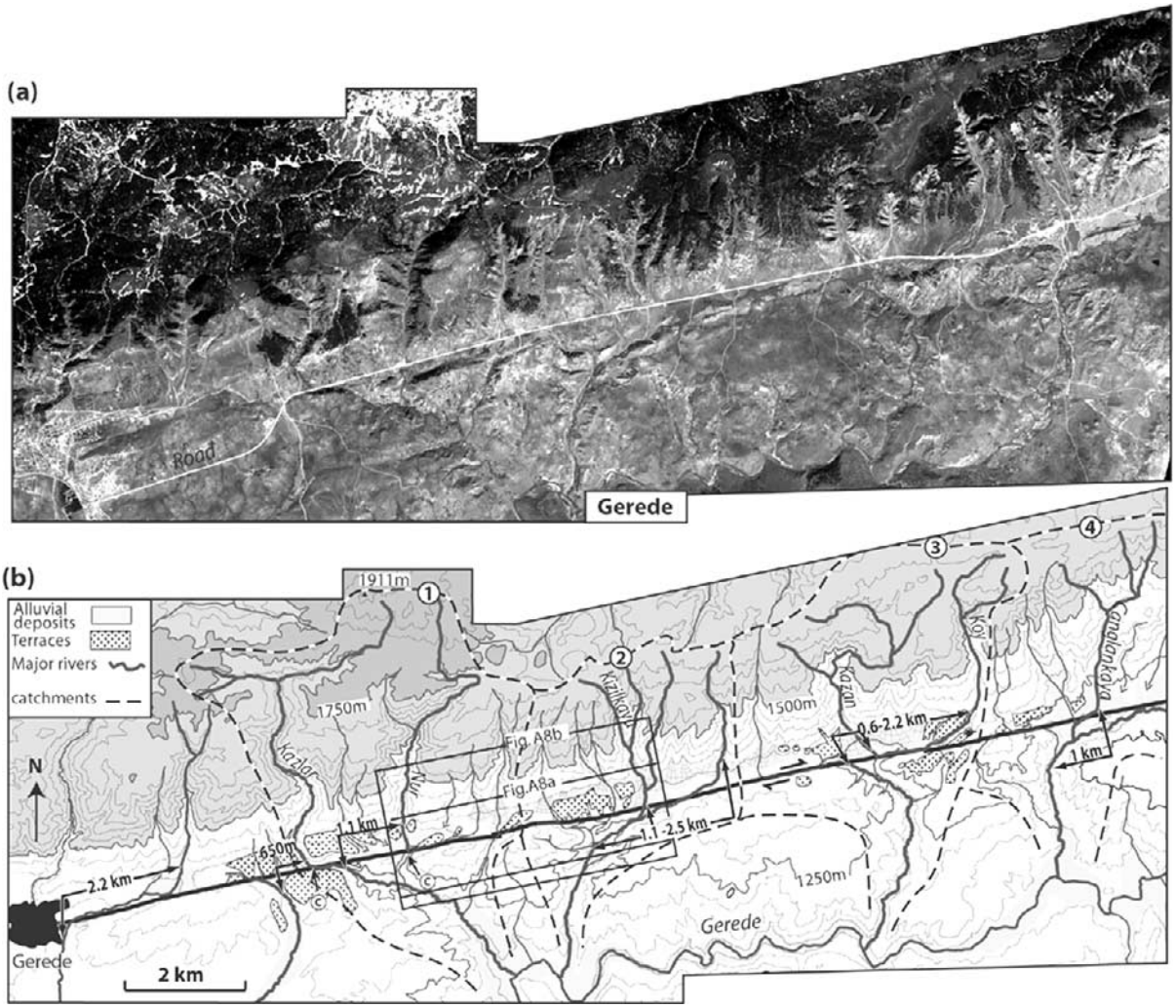

Figure A7. Kilometric drainage offsets in Gerede (see locations in Figure 7). (a) SPOT image. A white road runs close to the NAF trace east of Gerede. (b) Corresponding morphological map showing the trace of the NAF and the offset drainage (1:25,000 scale topography). Estimates of right-lateral valley offsets range from 0.6 to 2.2 km (see the double-headed arrows) along the fault trace. The southward directed drainage is deviated by shutter ridges along the edge of the southern block. The locations of Figure A8 are shown by boxes.

photograph interpretation, only the main river channels cross the fault depression covered by alluvial deposits (Figure A8). The Nur, Göç, Kavakli, and Kizilkaz rivers have enough stream power to incise the shutter ridges and go on flowing south of the fault toward the Gerede river. The whole morphology is offset across the fault. To the west, the Nur river has entrenched a valley that is filled by recent alluvium and its wrenched shape corresponds to a 115–140 m minimum offset (Figure A8a). The Göç river has a narrow channel that is twisted across the fault (Figure A8a). The river strike is oblique to the fault and we infer a minimum offset of about 125 m. To the east, the Kavakli river valley is straight across the fault, but its present geometry could result from a recent capture. An abandoned valley filled by young alluvium is located 180 ± 25 m more to the west, downstream the fault. This valley is beheaded by a 180-m-long shutter ridge. At the easternmost extremity of the study area, the Kizilkaya river incises a young alluvial surface and crosses the fault with no visible offset. On the western bank of the river, at least two terrace risers are visible south of the fault and the westernmost one is offset by about 135 m with respect to the present channel. In this area, the abandoned valley of the Kavakli river is the best preserved and clearest offset marker. Restoring the continuity of the Kavakli river with a 180-m left-lateral offset along the fault is compatible with the valley morphology of the three other main rivers (Figures A8b and A8c). In the restored stage the Nur river has a wide meandering valley covered by alluvium that is continuous across the fault, and the Göç river has a straight north-south channel (Figure A8c). More to the east, alluvium deposited in the Kizilkaya river valley forms a wide alluvial fan across the

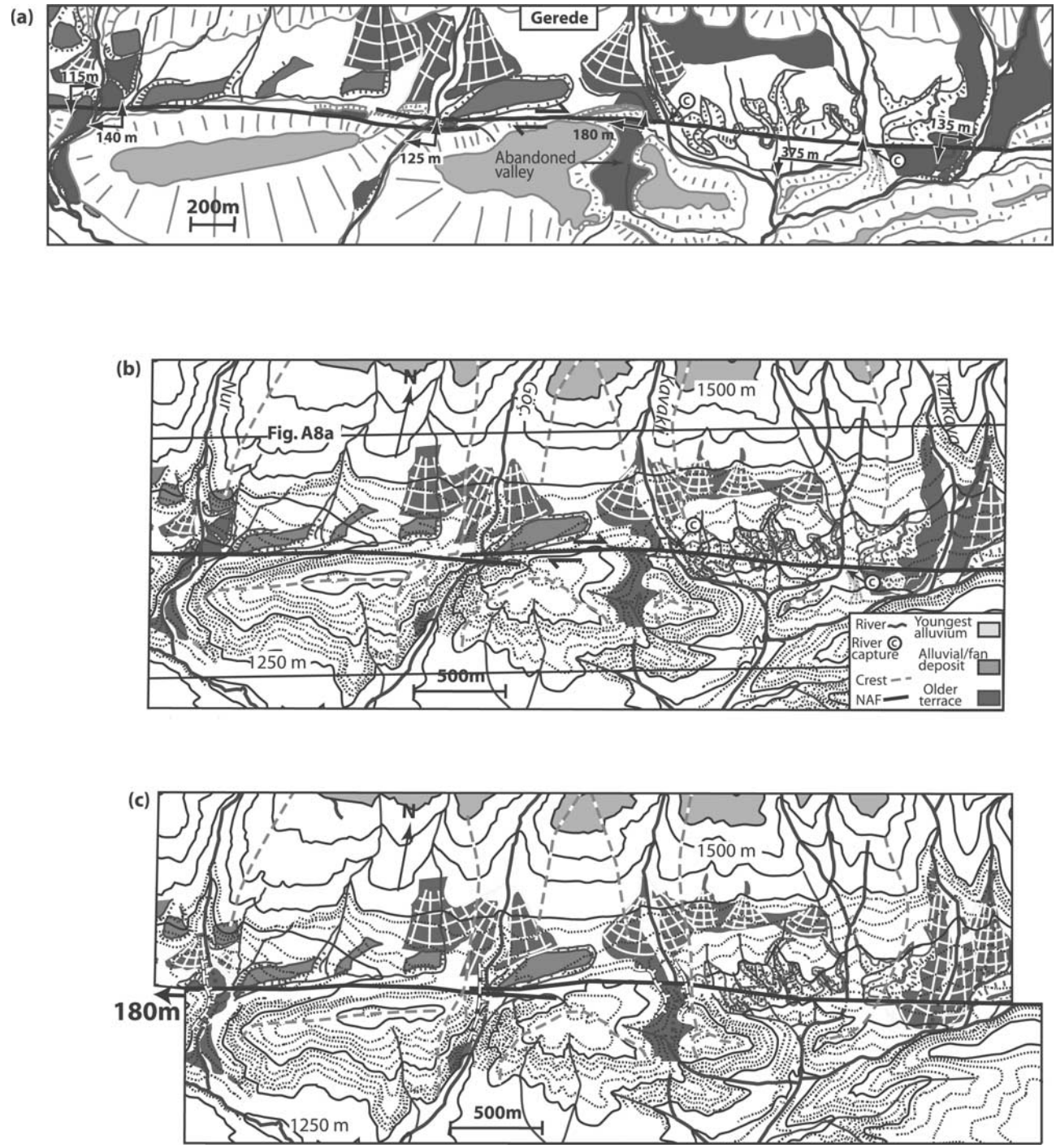

Figure A8. Detailed morphology of the NAF in Gerede (see location in Figure A7). (a) Interpretation of 1:10,000 scale aerial photographs. The large streams incise the fault zone and southern shutter ridges. Lateral offsets of these streams range from 115 to 180 m. An abandoned valley incised across the shutter ridges lies southwest of the Kavakli stream. Its apparent offset by the fault is 180 m. (b) Topography (at 1:25,000 scale, 10-m contour interval) with interpretation of an area that includes that shown in Figure A8a (outlined). (c) Restoration of offset features in Figure A8a by a back displacement of 180 m. The offsets of the paleochannel of the Kavakli river and of the other major rivers (Nur, Goc, and Kizilkaya rivers) are cancelled.

fault. The observed offsets of the incised valley morphology around Gerede appear to be similar to the one located more to the east in the Ilgaz Mountains, in Erzincan and in Destek. Note also that like in the Ilgaz and Erzincan areas, kilometric to tens meter offsets of catchments, river valley or terrace risers, occur along the same active fault trace that ruptured during the twentieth century earthquake sequence.

[60] **Acknowledgments.** Most of this work was done during the Ph.D. thesis of Aurélia Hubert-Ferrari [*Hubert-Ferrari*, 1998] under the

supervision of Rolando Armijo. The data bank of INSU-CNRS (program Tectoscope-Positionnement) gave us access to the satellite imagery. Field work was supported by a European community project organized by P. Bernard (contract EV5V-CT94-0513) and by CNRS. We thank J. Jackson for a constructive review.

References

Adyaman, O., Relations entre volcanisme et tectonique en contextes de collision et de Dècrochement (Turquie), Ph.D. thesis, 155 pp., Univ. of Cergy-Pontoise, Cergy-Pontoise, France, 2000.

Allen, C. R., Active faulting in northern Turkey, *Contrib. 1577*, 32 pp., Calif. Inst. of Technol., Div. of Geol. Sci., Pasadena, 1969.

Allen, C.R., Geological criteria for evaluating seismicity, *Geol. Soc. Am. Bull.*, *86*, 1041–1057, 1975.

Ambraseys, N. N., Some characteristic features of the North Anatolian Fault zone, *Tectonophysics*, *9*, 143–165, 1970.

Ambraseys, N. N., Temporary seismic quiescence: SE Turkey, *Geophys. J. R. Astron. Soc.*, *96*, 311–331, 1989.

Ambraseys, N. N., and C. F. Finkel, The Anatolian earthquake of 17 August 1668, in *Historical Seismograms and Earthquakes of the World*, edited by W. H. K. Lee, H. Meyers, and K. Shimazaki, pp. 173–180, Academic, San Diego, Calif., 1988.

Ambraseys, N. N., and A. Zatopek, The Mudurnu valley, western Anatolia, Turkey, earthquake of 22 July 1967, *Bull. Seismol. Soc. Am.*, *58*, 47–102, 1969.

Andrieux, J., S. Över, A. Poisson, and O. Bellier, The North Anatolian Fault Zone: Distributed Neogene deformation in its northward convex part, *Tectonophysics*, *243*, 135–154, 1995.

Armijo, R., B. Meyer, G. C. P. King, A. Rigo, and D. Papanastassiou, Quaternary evolution of the Corinth rift and its implications, *Geophys. J. Int.*, *126*, 11–53, 1996.

Armijo, R., B. Meyer, A. Hubert-Ferrari, and A. A. Barka, Propagation of the North Anatolian fault into the northern Aegean: Timing and kinematics, *Geology*, *27*, 267–270, 1999.

Arpat, E., and F. Şaroglu, The east Anatolian fault system: Thoughts on its development, *Bull. Miner. Res. Explor. Inst. Turk.*, *78*, 33–39, 1972.

Aydin, A., and A. Nur, Evolution of pull-apart basins and their scale independence, *Tectonics*, *1*, 91–105, 1982.

Barka, A. A., Geology and tectonic evolution of some Neogene-Quaternary basins in the North Anatolian fault zone, special publication, pp. 209–227 *Geol. Soc. of Turk.*,, 1984.

Barka, A. A., The North Anatolian fault zone, *Ann. Tecton.*, suppl. 6, 164–195, 1992.

Barka, A. A., Slip distribution along the North Anatolian fault associated with the large earthquakes of the period 1939 to 1967, *Bull. Seismol. Soc. Am.*, *86*, 1238–1254, 1996.

Barka, A. A., and L. Gülen, New constraints on age and total offset of the North Anatolian Fault Zone: Implications for tectonics of the eastern Mediterranean region, *Middle East Tech. Univ. J. Pure Appl. Sci.*, *31*, 39–63, 1988.

Barka, A. A., and L. Gülen, Complex evolution of the Erzincan Basin (eastern Turkey), *Tectonophysics*, *11*, 275–283, 1989.

Barka, A. A., and P. L. Hancock, Neotectonic deformation patterns in the convex-northwards arc of the North Anatolian fault, in *The Geological Evolution of the eastern Mediterranean*, edited by J. G. Dixon and A. H. F. Robertson, *Spec. Publ. Geol. Soc*, *17*, 763–773, 1984.

Barka, A. A., and K. Kadinsky-Cade, Strike-slip fault geometry in Turkey and its influence on earthquake activity, *Tectonophysics*, *7*, 663–684, 1988.

Bergougnan, H., Relations entre les édifices pontiques et tauriques dans le nord-est de l'Anatolie, *Bull. Soc. Geol. Fr.*, *17*, 1045–1057, 1975.

Bingöl, E., Geological map of Turkey, scale 1:2,000,000, Gen. Dir. of Miner. Res. and Explor., Ankara, 1989.

Bottema, S., The late glacial in the eastern Mediterranean and the near East, in *The Environmental History of the Near and Middle East Since the Last Ice Age*, edited by W. C. Brice, pp. 15–28, Academic, San Diego, Calif., 1978.

Bournes, S. J., P. C. England, and B. Parsons, The motion of crustal blocks driven by flow of the lower lithosphere and implications for slip rates of continental strike-slip faults, *Nature*, *391*, 655–659, 1998.

Bozkurt, E., and A. Koçygit, The Kazova basin: An active negative flower structure on the Almus fault zone, a splay fault system of the North Anatolian Fault Zone, Turkey, *Tectonophysics*, *265*, 239–254, 1996.

Brakenridge, G. R., Widespread episodes of stream erosion during Holocene and their climatic cause, *Nature*, *283*, 655–656, 1980.

Brice, W. C., The desiccation of Anatolia, in *The Environmental History of the Near and Middle East Since the Last Ice Age*, edited by W. C. Brice, pp. 141–147, Academic, San Diego, Calif., 1978.

Bull, W. B., *Geomorphic Responses to Climatic Change*, 326 pp., Oxford Univ. Press, New York, 1991.

Degens, E. T., and T. Kurtman, The geology of Lake Van, *Bull. Miner. Res. Explor. Inst. Turk.*, *169*, 158 pp., 1978.

Deweys, J. W., Seismicity of northern Anatolia, *Bull. Seismol. Soc. Am.*, *66*, 843–868, 1976.

Dirik, K., Geological history of the northward arched segment of the North Anatolian transform fault zone, *Geol. J.*, *28*, 251–266, 1993.

England, P., and D. McKenzie, A thin viscous sheet model for continental deformation, *Geophys. J. R. Astron. Soc.*, *70*, 295–321, 1982.

Erinc, S., Changes in the physical environment in Turkey since the end of the last glacial, in *The Environmental History of the Near and Middle East Since the Last Ice Age*, edited by W. C. Brice, pp. 87–110, Academic, San Diego, Calif., 1978.

Erol, O., The quaternary history of the lake basins of central and southern Anatolia, in *The Environmental History of the Near and Middle East Since the Last Ice Age*, edited by W. C. Brice, pp. 111–139, Academic, San Diego, Calif., 1978.

Fuenzalida, H., L. Dorbath, A. Cisternas, A. Rivera, H. Haessler, H. Philip, A. Barka, and H. Eyidogan, Mechanism of the 1992 Erzincan earthquake and its aftershocks, tectonics of the Erzincan Basin and decoupling on the North Anatolian Fault, *Geophys. J. Int.*, *129*, 1–28, 1997.

Gaudemer, Y., P. Tapponnier, and D. L. Turcotte, River offsets across active strike-slip faults, *Ann. Tecton.*, *3*, 55–76, 1989.

Harrison, S. P., I. C. Prentice, and P. J. Bartlein, Influence of insolation and glaciation on atmospheric circulation in the North Atlantic sector: Implications of general circulation model experiments for the late Quaternary climatology of Europe, *Quat. Sci. Rev.*, *11*, 283–299, 1992.

Hempton, M. R., and L. A. Dunne, Sedimentation in pull-apart basins: Active example in eastern Turkey, *J. Geol.*, *92*, 513–530, 1984.

Houseman, G., and P. England, Finite strain calculations of continental deformation, 1, Method and general results for convergent zone, *J. Geophys. Res.*, *99*, 3651–3663, 1986.

Hubert-Ferrari, A., La faille Nord-Anatolienne (cinématique, morphologie, localisation, vitesse et décalage total) et modélisations utilisant la contrainte de Coulomb sur différentes échelles de temps, Ph.D. thesis, 222 pp., Univ. of Paris VII-Denis Diderot Univ., Paris, 1998.

Hubert-Ferrari, A., A. Barka, E. Jacques, S. Nalbant, B. Meyer, R. Armijo, P. Tapponnier, and G. C. P. King, Seismic hazard in the Sea of Marmara following the Izmit earthquake, *Nature*, *404*, 269–273, 2000.

Hubert-Ferrari, A., G. C. P. King, I. Maniguetti, R. Armijo, and P. Tapponnier, First order elastic modelling of the Aden ridge propagation and the Anatolian extrusion process, *Geophys. J. Int.*, in press, 2002.

Irrlitz, W., Lithostratigraphic und tektonische Entwicklung des Neogens in Nordostanalien, *Geol. Jahrb. Beih.*, *120*, 1–111, 1972.

Jackson, J., Active tectonics of the Aegean region, *Annu. Rev. Earth Planet. Sci.*, *22*, 239–271, 1994.

Jackson, J., and D. P. McKenzie, Active tectonics of the Alpine Himalayan belt between western Turkey and Pakistan, *Geophys. J. R. Astron. Soc.*, *77*, 185–264, 1984.

Jackson, J., and D. P. McKenzie, The relationship between plate motion and seismic moment tensors, and the rates of active deformation in the Mediterranean and Middle East, *Geophys. J.*, *93*, 45–73, 1988.

Jackson, J., J. W. Haines, and W. E. Holt, The horizontal velocity field in the deforming Aegean Sea region determined from the moment tensors of earthquakes, *J. Geophys. Res.*, *97*, 17,657–17,684, 1992.

Julien, P. Y., *Erosion and Sedimentation*, 280 pp., Cambridge Univ. Press, New York, 1995.

Ketin, I., Über die tektonish-mechanischen Folgerungen aus den grossen anatolischen Erbeben des letzten Dezenniums, *Geol. Rundsch.*, *36*, 77–83, 1948.

Ketin, I., About the strike-slip movement of North Anatolia (in German), *Bull. Miner. Res. Explor. Inst. Turk.*, *72*, 1–28, 1969.

Knox, J. C., Fluvial responses to small-scale climatic changes, in *Developments and Applications of Geomorphology*, edited by J. E. Costa and P. J. Fleisher, pp. 318–342, Springer-Verlag, New York, 1984.

Koçyigit, A., Susehri basin: An active fault wedge basin, *Tectonophysics*, *167*, 13–29, 1989.

Koçyigit, A., Tectonic setting of the Gölova basin: Total offset of the North Anatolian Fault zone, E. Pontide, Turkey, *Ann. Tecton.*, *2*, 155–170, 1990.

Lacassin, R., A. Replumaz, and P. H. Leloup, Hairpin river loops and slip-sense inversion on southeast Asian strike-slip faults, *Geology*, *26*, 703–706, 1998.

Lambeck, K., Late Pleistocene and Holocene sea-level change in Greece and south-western Turkey; a separation of eustatic, isostatic and tectonic contributions, *Geophys. J. Int.*, *122*, 1022–1044, 1995.

Landmann, G., A. Reimer, G. Lemcke, and S. Kempe, Dating late glacial abrupt climate change in the 14570 years long continous varve record of Lake Van, Turkey, *Palaeogeogr. Palaeoclimatol. Palaeoecol.*, *122*, 107–118, 1996.

Lautenschlager, M., and K. Herterich, Atmospheric response to ice age

conditions: Climatology near the Earth's surface, *J. Geophys. Res.*, *95*, 22,547–22,557, 1990.
Le Pichon, X., and J. Angelier, The Aegean Sea, *Philos. Trans. R. Soc. London, Ser. A.*, *300*, 357–372, 1981.
McClusky, S., et al., Global Positioning System constraints on plate kinematics and dynamics in the eastern Mediterranean and Caucasus, *J. Geophys. Res.*, *105*, 5695–5719, 2000.
McKenzie, D. P., Active tectonics of the Mediterranean region, *Geophys. J. R. Astron. Soc.*, *30*, 109–185, 1972.
McKenzie, D. P., Active tectonics of the Alpine-Himalaya belt: The Aegean Sea and surrounding regions, *Geophys. J. R. Astron. Soc.*, *55*, 217–254, 1978.
Merrits, D. J., and K. R. Vincent, Geomorphic response of coastal stream to low, intermediate, and high rates of uplift, Mendocino triple junction region, northern California, *Geol. Soc. Am. Bull.*, *101*, 1373–1388, 1995.
Meyer, B., P. Tapponnier, L. Bourjot, F. Métivier, Y. Gaudemer, and G. Peltzer, Guo Shunmin, and Chen Zhitai, Crustal thickening in Gansu-Qinghai, lithospheric mantle subduction, and oblique, strike slip controlled growth of the Tibet Plateau, *Geophys. J. Int.*, *135*, 1–47, 1998.
Molnar, P., et al., Continuous deformation versus faulting through the continental lithosphere of New Zealand, *Science*, *286*, 516–519, 1999.
Nalbant, S. S., A. Hubert, and G. C. P. King, Stress coupling between earthquakes in Northwest Turkey and the north Aegean Sea, *J. Geophys. Res.*, *103*, 24,469–24,486, 1998.
Öcal, N., 1957 Abant earthquake, seismological publication, 70 pp., Kandilli Obs., Istanbul, 1959.
Okay, A. I., and O. Sahinturk, Geology of the eastern Pontides, in *Regional and Petroleum Geology of the Black Sea and Surrounding Region*, edited by A. G. Robinson, *AAPG Mem.*, *68*, 291–311, 1997.
Över, S., Analyse tectonique et états de contrainte cénozoiques dans la zone centrale de la faille Nord-Anatolienne, Ph.D thesis, Univ. of Paris-Sud, Orsay, France, 1996.
Över, S., O. Bellier, A. Poisson, J. Andrieux, and Z. Tutkun, Esquisse de l'évolution néogène à actuelle de l'état de contrainte dans la partie centrale de la faille Nord Anatolienne (Turquie), *C. R. Acad. Sci., Ser. 2*, *317*, 827–833, 1993.
Prentice, I. C., J. Guiot, and S. P. Harrisson, Mediterranean vegetation, lake levels and palaeoclimate at the Last Glacial Maximum, *Nature*, *360*, 658–660, 1992.
Reilinger, R. E., S. C. McClusky, M. B. Oral, R. W. King, M. N. Toksoz, A. A. Barka, I. Kinik, O. Lenk, and I. Sanli, Global Positioning System measurements of the present-day crustal movements in the Arabia-Africa-Eurasia plate collision zone, *J. Geophys. Res.*, *102*, 9983–9999, 1997.
Replumaz, A., R. Lacassin, P. Tapponnier, and P. H. Leloup, Large river offsets and Plio-Quaternary dextral slip rate on the Red River fault (Yunnan, China), *J. Geophys. Res.*, *106*, 819–836, 2001.
Roberts, N., Age, palaeoenvironments, and climatic significance of late Pleistocene Konya Lake, Turkey, *Quat. Res.*, *19*, 154–171, 1983.
Roberts, N., and H. E. Wright Jr., Vegetational, lake-level, and climatic history of the near east and Southwest Asia, in *Global Climates Since the Last Glacial Maximum*, edited by H. E. Wright Jr. et al., pp. 194–220, Univ. of Minn. Press, Minneapolis, 1993.
Rogl, V. F., and F. F. Steininger, Vom Zerfall der Tethys zu Mediterran und Paratethys-die Neogene Paleogeographie und Palinplastik des antikem Mediterranschen Raumes, *Ann. Naturhist. Mus. Wien*, *85*, 135–163, 1983.
Şaroglu, F., Age and offset of the North Anatolian Fault, *Middle East Tech. Univ. J. Pure Appl. Sci.*, *31*, 65–79, 1988.
Scholz, C. H., N. H. Dawers, J.-Z. Yu, M. H. Anders, and P. A. Cowie, Fault growth and fault scaling laws: Preliminary results, *J. Geophys. Res.*, *98*, 21,951–21,961, 1993.
Schumm, S. A., *The Fluvial System*, 338 pp., Wiley-Interscience, New York, 1977.
Schumm, S. A., Alluvial river response to active tectonics, in *Active Tectonics*, pp. 80–94, Natl. Acad. Press, Washington, D. C., 1986.
Sengör, A. M. C., The north Anatolian transform fault: Its age offset and tectonic significance, *J. Geol. Soc. London*, *136*, 269–282, 1979.
Sengör, A. M. C., and A. A. Barka, Evolution of escape-related strike-slip systems: Implication for distributions of collisional orogens (abstract), *Proc. Int. Geol. Congr.*, *29*, 232, 1992.
Sengör, A. M. C., N. Görür, F. Şaroglu. Strike-slip faulting and related basin formation in zones of tectonic escape: Turkey as a case study, in *Strike-Slip Faulting and Basin Formation*, edited by K. T. Biddle and N. Christie-Blick, *Spec. Publ. Soc. Econ. Paleontol. Mineral.*, *37*, 227–267, 1985.
Seymen, I., Kelkit vadisie kesiminde Kusey Anadolu Fay Aonunun tektonik ozelligi, Yay thesis, 192 pp., Istanbul Tek.-Univ. Maden Fak., Istanbul, 1975.
Stanley, D. J., and C. Blanpied, Late Quaternary water exchange between the eastern Mediterranean and the Black Sea, *Nature*, *285*, 537–541, 1980.
Stein, R. S., A. A. Barka, and J. H. Dieterich, Progressive failure on the North Anatolian fault since 1939 by earthquake triggering, *Geophys. J. Int.*, *128*, 594–604, 1997.
Straub, C., H. G. Kahle, and C. Schindler, GPS and geological estimates of the tectonic activity in the Marmara Sea region, NW Anatolia, *J. Geophys. Res.*, *102*, 27,587–27,601, 1997.
Tapponnier, P., G. Peltzer, A. Y. Le Dain, A. Armijo, and P. Cobbold, Propagating extrusion tectonics in Asia: New insights from simple experiments with plasticine, *Geology*, *10*, 611–616, 1982.
Tatar, O., J. D. A. Piper, R. G. Park, and H. Gürsoy, Paleomagnetic study of block rotations in the Niksar overlap region of the North Anatolian Fault Zone, central Turkey, *Tectonophysics*, *244*, 251–266, 1995.
Taymaz, T., J. Jackson, and D. McKenzie, Active tectonics of the north and central Aegean Sea, *Geophys. J. Int.*, *106*, 537–550, 1991.
Ünay, E., and H. de Bruijn, Plio-Pleistocene rodents and lagomorphs from Anatolia, in *The Dawn of the Quaternary, Proceedings of the SEQS-EuroMam Symposium, 1996, Meded. 60*, pp. 431–462, Ned. Inst. voor Toegepaste Geowet. TNO, Delft, Netherlands, 1998.
Vilotte, J. P., M. Daignières, and R. Madariaga, Numerical modeling of intraplate deformation: Simple mechanical models of continental collision, *J. Geophys. Res.*, *87*, 10,709–10,728, 1982.
Wallace, R. E., Notes on stream channels offset by the San Andreas Fault, southern Coast Ranges, *Stanford Univ. Publ. Geol. Sci.*, *11*, 6–20, 1968.
Westaway, R., Present-day kinematics of the Middle East and eastern Mediterranean, *J. Geophys. Res.*, *99*, 12,071–12,090, 1994.
Yilmaz, A., Basic geological characteristics and structural evolution of the region between Upper Kelkit stream and Munzur Mountains (in Turkish), *Bull. Geol. Soc. Turk.*, *28*, 79–92, 1985.
Yilmaz, Y., E. Yigitbas, and S. C. Gens, Ophiolitic and metamorphic assemblages of southeast Anatolia and their significance in the geological evolution of the orogenic belt, *Tectonics*, *12*, 1280–1297, 1993.
Yilmaz, Y., O. Tuysuz, E. Yigitbas, S. C. Genc, and A. M. C. Sengör, Geology and tectonic evolution of the Pontides, in *Regional and Petroleum Geology of the Black Sea and Surrounding Region*, edited by A. G. Robinson, *AAPG Mem.*, *68*, 183–226, 1997.

A. Hubert-Ferrari, Institut de Géologie, Université de Neuchâtel, CH-2007 Neuchâtel, Switzerland. (aurelia.ferrari@unine.ch)
G. C. P. King, B. Meyer, and R. Armijo, Laboratoire de Tectonique, Mécanique de la Lithosphère (UMR 7578 of CNRS), Institut de Physique du Globe de Paris, 4 Place Jussieu, F-75252 Paris Cedex 05, France. (king@ipgp.jussieu.fr; meyer@ipgp.jussieu.fr; rolando@ipgp.jussieu.fr)
A. Barka, Eurasian Earth Sciences Institute, ITU, Ayazaga, 80626 Istanbul, Turkey.